REPORT DOCUMENTATION PAGE

Form Approved
OMB No. 0704-0188

1. AGENCY USE ONLY (Leave blank)	2. REPORT DATE	3. REPORT TYPE AND DATES COVERED
	31 May 1995	Summary 01 Jun 94 - 31 May 95

4. TITLE AND SUBTITLE
Fundamental Studies of Radial Wave Thermoacoustic Engines

5. FUNDING NUMBERS
PE 61153N
G N0001493 J 1131
TA 3126975ess

6. AUTHOR(S)
W. Patrick Arnott

7. PERFORMING ORGANIZATION NAME(S) AND ADDRESS(ES)
Atmospheric Sciences Center
Desert Research Institute
P.O. Box 60220
Reno, NV 89506-0220

8. PERFORMING ORGANIZATION REPORT NUMBER

9. SPONSORING/MONITORING AGENCY NAME(S) AND ADDRESS(ES)
Office of Naval Research
ONR 331
800 North Quincy Street
Arlington, VA 22217-5660

10. SPONSORING/MONITORING AGENCY REPORT NUMBER

11. SUPPLEMENTARY NOTES

12a. DISTRIBUTION/AVAILABILITY STATEMENT
Approved for public release:
Distribution unlimited

12b. DISTRIBUTION CODE

13. ABSTRACT (Maximum 200 words)

Our research is about arbitrary geometry thermoacoustic engines. The specific geometry studied in detail is the radial wave arrangement. Formal theory and the short stack approximation were derived for this geometry and were used to pursue an answer to the following question: Radial or plane wave thermoacoustic refrigerators? To date, the plane wave refrigerator appears to be the best overall compromise refrigerator, though the radial wave refrigerator has a higher cooling capacity. An evolving numerical design program has been enhanced to include radial or plane wave engines with variable plate spacing and both plane and radial wave resonators simultaneously with application to driving radial wave refrigerators with heat driven plane wave sound sources. Our experiments have mainly been aimed at radial wave prime movers for the purposes of validating the theory and investigating the large amplitude behavior. Heat exchanger design is a critical issue.

14. SUBJECT TERMS	15. NUMBER OF PAGES
Thermoacoustic, refrigeration, Heat-Driven Sound Source, Radial Geometry	61
	16. PRICE CODE

17. SECURITY CLASSIFICATION OF REPORT	18. SECURITY CLASSIFICATION OF THIS PAGE	19. SECURITY CLASSIFICATION OF ABSTRACT	20. LIMITATION OF ABSTRACT
UNCLASSIFIED	UNCLASSIFIED	UNCLASSIFIED	

Progress Report for

FUNDAMENTAL STUDIES OF RADIAL WAVE THERMOACOUSTIC ENGINES

June 1995

by
W. Patrick Arnott
Atmospheric Sciences Center
Desert Research Institute
PO Box 60220
Reno NV 89506

for
Dr. Logan E. Hargrove
and
The Navy Environmentally Safe Ships Program

ABSTRACT

Our research is about arbitrary geometry thermoacoustic engines. The specific geometry studied in detail is the radial wave arrangement. Formal theory and the short stack approximation were derived for this geometry and were used to pursue an answer to the following question: Radial or plane wave thermoacoustic refrigerators? To date, the plane wave refrigerator appears to be the best overall compromise refrigerator, though the radial wave refrigerator has a higher cooling capacity.

An evolving numerical design program has been enhanced to include radial or plane wave engines with variable plate spacing and both plane and radial wave resonators simultaneously with application to driving radial wave refrigerators with heat driven plane wave sound sources.

Our experiments have mainly been aimed at radial wave prime movers for the purposes of validating the theory and investigating the large amplitude behavior. Heat exchanger design is a critical issue.

Progress Report for

FUNDAMENTAL STUDIES OF RADIAL WAVE THERMOACOUSTIC ENGINES

TABLE OF CONTENTS

1. Project Description The goal of our research (in close collaboration with Richard Raspet and students from the Univ. MS) is to determine the merits of alternative geometry thermoacoustic refrigerators. A brief review of standard plane wave thermoacoustic refrigerators will set the stage for the discussion of alternative geometry refrigerators. The intuitive aspects of thermoacoustic refrigeration have been developed as a result of the short stack approximation for thermoacoustics.[1,2] Figure 1 shows schematically a typical plane wave refrigerator. The sound source stimulates heat flow up the temperature gradient formed across the stack plates. The plates are spaced by a few thermal boundary layers, δ_κ, though since δ_κ depends on temperature, the plate spacing is not optimal at all point along the stack. The distribution of kinetic, potential, and thermoacoustic power is also shown in Fig. 1 for standing waves. At first glance it appears that the stack should be placed at a peak for thermoacoustic power to maximize refrigeration. However, when efficiency (or more properly, Coefficient of Performance, COP) is important, some thermoacoustic power can be sacrificed to save on kinetic energy dissipation due to gas viscosity and friction from the relative motion of the stack and gas.

Suppose that the resonator in Figure 1 could be contorted into any shape, perhaps an exponential or conical horn shape, and suppose that the plate spacing could be made arbitrary at any position along the resonator. An example of such a resonator is shown in Fig. 2. Does a resonator and stack geometry exist that will greatly improve upon the performance of plane wave refrigerators? What properties of alternative geometry thermoacoustic engines change on account of the contortion? The distributions of potential and kinetic energy dissipation, and of thermoacoustic power generation, are altered by geometry, as is the relation between optimal thermal boundary layer thickness and stack plate spacing. Formal analysis for arbitrary geometry thermoacoustics is performed using our previous theory[3] with a new differential equation for specific acoustic impedance for the stack.[4]

1. Why study alternative geometry acoustic refrigerators?

Plane Wave Thermoacoustics
(standard)

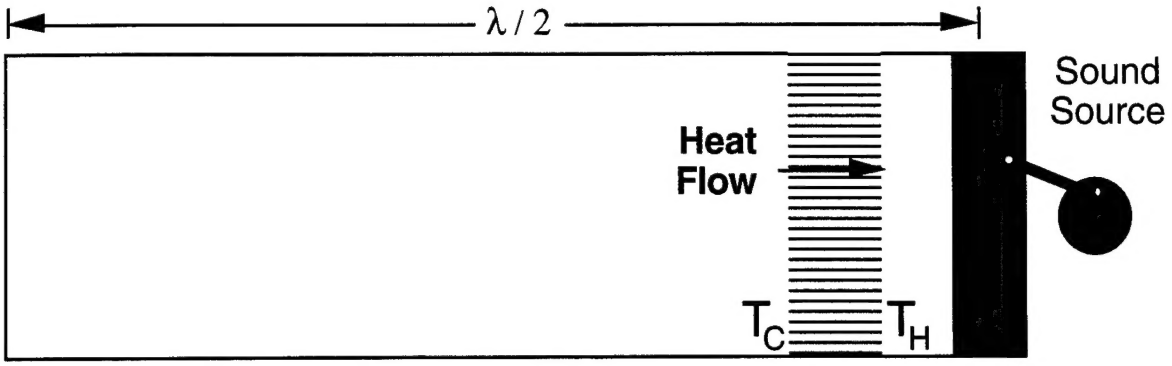

Optimal Spacing ≈ 2.5 $\delta\kappa$
but ...

($\delta\kappa$ is the distance heat can travel during one sound source oscillation)

$\delta\kappa$ depends on T
($\delta\kappa \propto T^{0.83}$ for He)

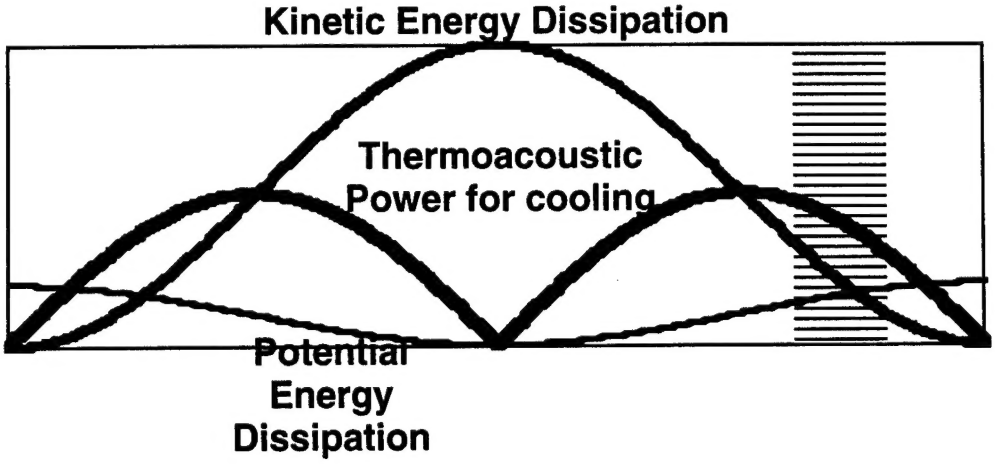

Figure 1. Standard geometry acoustic refrigerator.

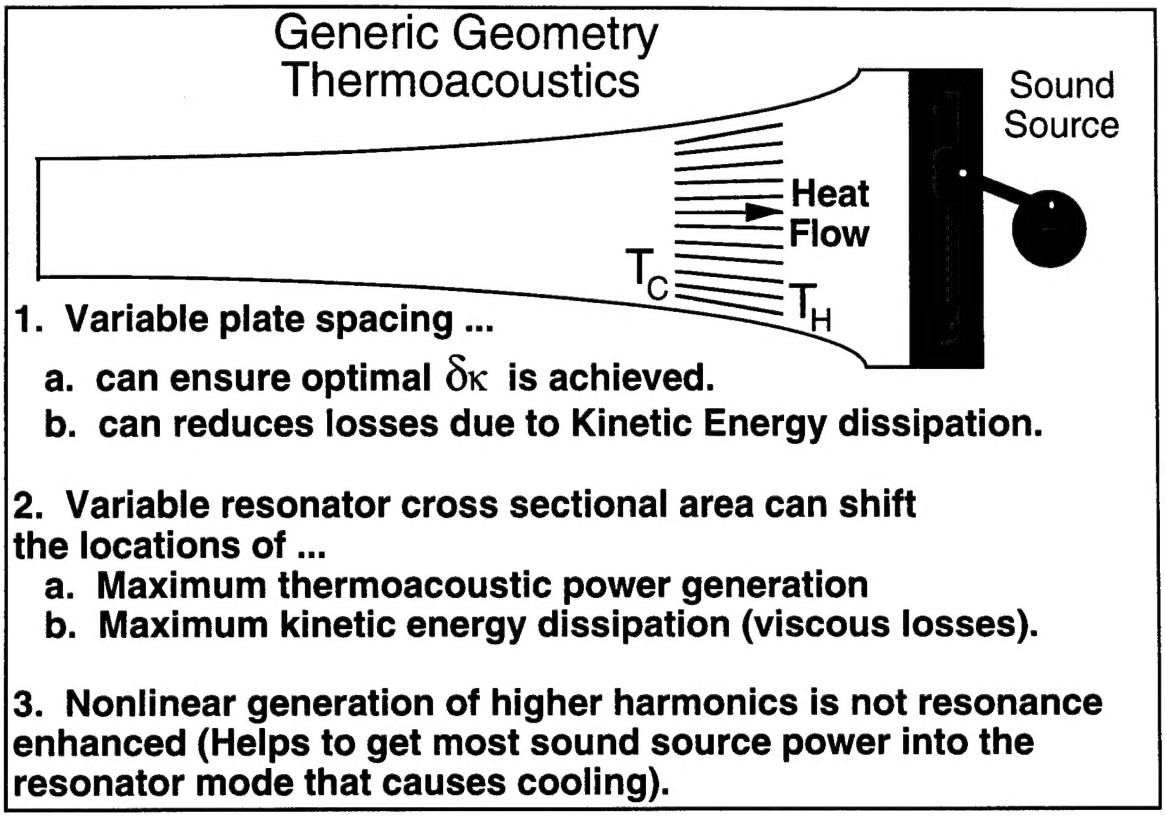

Figure 2. Generic geometry thermoacoustic refrigerator.

The Hofler low-loss resonator design, and the use of a bulb at the quarter wavelength location of a resonator to give a low impedance are examples of resonators that deviate from the strictly plane form. Bennett[5] studied variable plate spacing refrigeration, though her formulation was somewhat incomplete.[4] She found improvement of the refrigerator COP when the stack plates are flared wider at the hot end.

The specific geometry we have considered in detail is the radial wave geometry[2] shown in Fig. 3. Note that there are two possible stack locations in this geometry. We developed a specific theoretical methodology for this geometry,[2] though we later found it was a special case of the arbitrary geometry method.[4] Jay Lightfoot, a student at the University of Mississippi, is currently working on a radial wave prime mover.

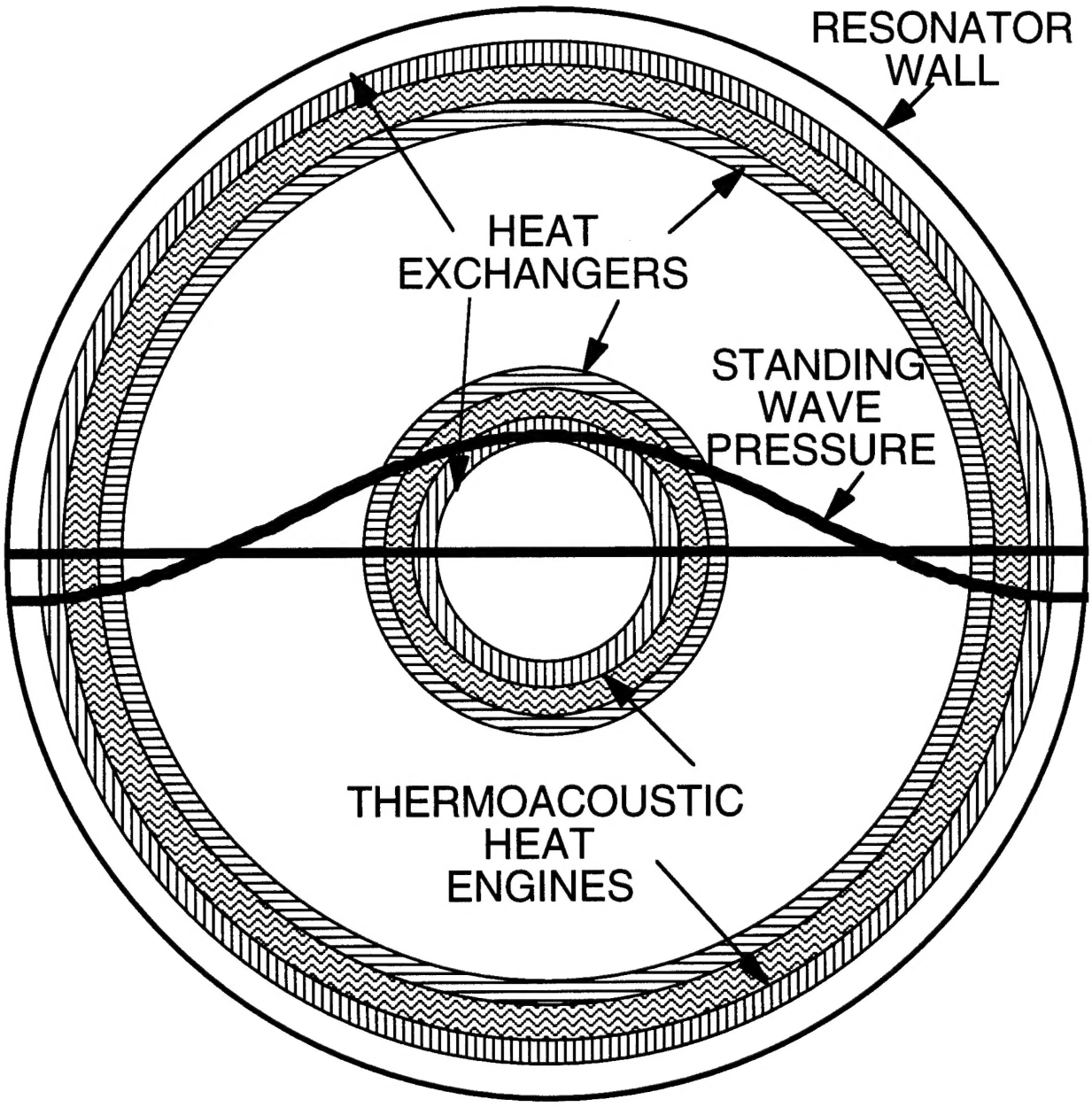

Figure 3. Radial wave geometry thermoacoustic engine.

2. Approach taken.

Our approach has been to investigate in detail a specific example, the radial wave geometry, as a non plane wave thermoacoustic engine.[2] We have developed a numerical design code for prime movers, and are finishing the code modifications for refrigerators and heat driven prime movers that generate the sound for acoustic

refrigerators. The code will allow for mixed mode geometries (i.e. radial and plane wave resonators) in the same system. We are currently seeking experimental validation of our code and theory through the development and testing of a radial wave prime mover.

Only recently we realized that a more general formulation for arbitrary engines was possible, and that this general form contained the radial wave problem as a special case. The numerical implementation of this theory is currently underway (prime movers in MS, refrigerators and prime movers together at DRI).

3. Specific work accomplished, June 1994 - May 1995.

3a. Theory.

We have completed a thorough theoretical analysis for radial wave thermoacoustic engines, and have used the short stack approximation of thermoacoustic to compare the theoretical promise of such engines.[2] Our short stack analysis assumes nominally standing waves in the resonator. I will distill the most pertinent results from our analysis (the formal publication should be available soon: the preprint is included as Appendix 1).

Thermoacousticians early on found[1] that acoustic refrigerators could develop a large cooling capacity, though at the expense of efficiency or Coefficient of Performance (COP). Thus we developed a Coefficient of Compromise, C_m, as follows:

$$C_m \equiv \left(\frac{COP}{COPc} \right)^m |\bar{\dot{Q}}_2(\phi)| \quad , \quad (m \geq 0) \quad , \tag{1}$$

where COPc is the highest possible, or Carnot Coefficient of Performance,[1] and $|\bar{\dot{Q}}_2(\phi)|$ is the cooling capacity of the refrigerator. For example, when m=1, cooling capacity and COP are equally emphasized, when m<1, cooling capacity is emphasized more than COP, and when m>1, COP is emphasized more than cooling capacity.

Figure 4 shows cooling capacity and COP as a function of the emphasis power, m, in Eq. (1), for 'equivalent' radial and plane wave acoustic refrigerators and for an efficient gas mixture with low Prandtl number. Each refrigerator was optimized with

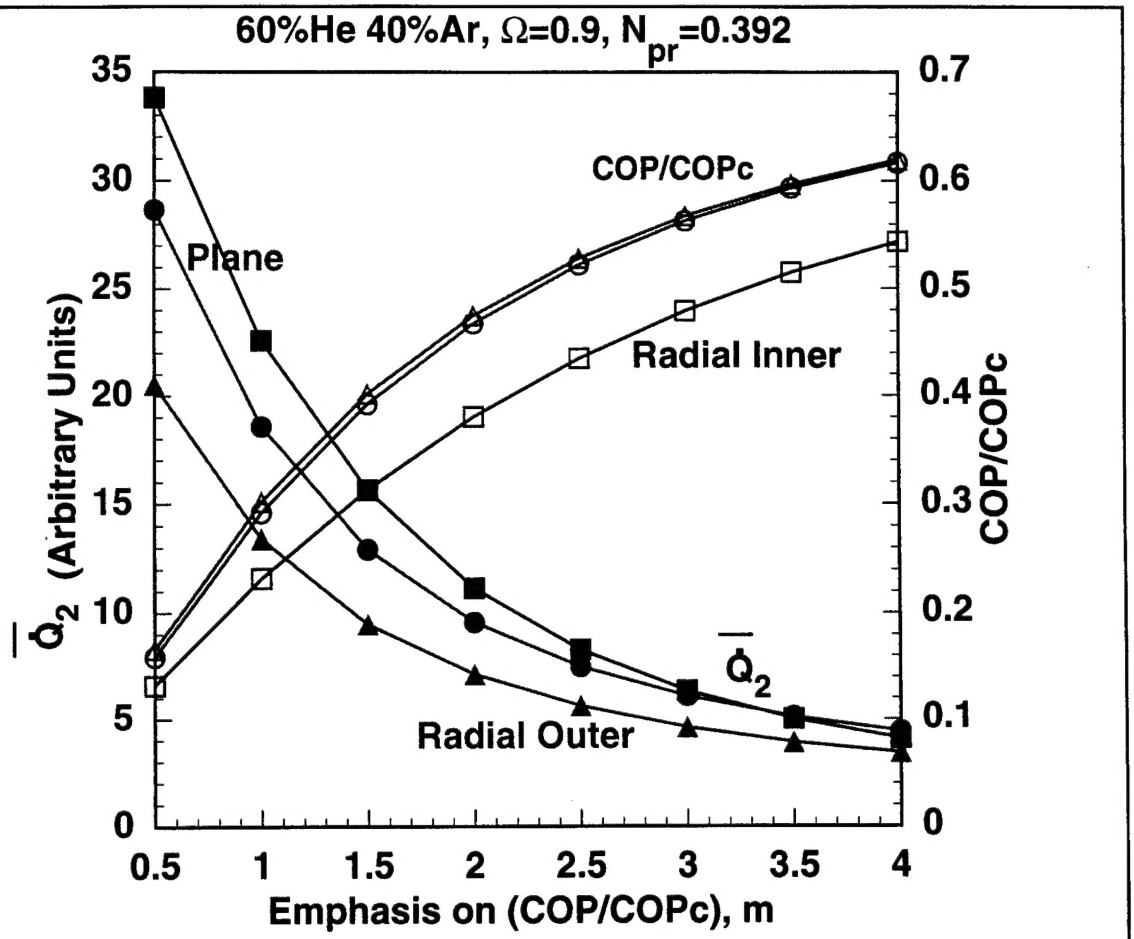

Figure 4. Compromise for plane and radial wave thermoacoustic refrigerators. Radial inner is given by the squares, radial outer by the triangles, and plane by circles. Open symbols are COP/COPc, and solid symbols are cooling capacity.

respect to maximizing C_m by adjusting the stack plate spacing, location in the standing wave, and stack length. Details can be found in Appendix 1. At low m, cooling capacity is emphasized over COP, and radial wave inner refrigerators have the highest cooling capacity and lowest COP/COPc. The COP/COPc ratio is very similar for plane and radial outer refrigerators, though the plane case has a greater cooling capacity. At large m, where COP/COPc is emphasized, plane wave refrigerators have highest cooling capacity and COP/COPc. For cooling capacity alone, the radial inner refrigerator is probably the choice to make, though plane wave acoustic refrigerators are generally best overall compromise refrigerators. I emphasize that the results reported in Fig. 4

were performed using the short stack approximation of thermoacoustics; the same analysis should be performed, at least in part, using the full theory and numerical implementation thereof.

3b. Experiment

Jay Lightfoot, a Ph.D. student at the University of Mississippi, is currently working on a radial wave prime mover. The purposes of this experiment are to validate the numerical model, and to investigate the structure of harmonics that develop at high amplitude. Since resonator modes are not even close to being the same frequency as most harmonics, it is expected that this geometry will result in more energy in the fundamental than equivalent plane wave resonators. Our contribution to this work is in design and construction of heat exchangers. Figure 5 shows one of the heat exchangers manufactured at DRI.

Jay is using silicon bonded mica paper stack material which has a thermal conductivity of 0.17 W/(m K) at room temperature, compared to 0.2 W/(m K) for Kapton, another material frequently used in stack construction. Low thermal conductivity stack material is desirable since it minimizes the normal heat flow down the temperature gradient. Mica paper is frequently used in toasters, and is much stiffer than Kapton for equivalent thicknesses. We are also using the mica paper in our prime movers for the thermoacoustic enhanced photoacoustic spectrometer at DRI.

Heat transfer and heat exchangers in thermoacoustics play an extremely important role in the overall success of a practical device. Any number of books have been written on heat transfer, for example Ref. 6 from which the following discussion is derived. The discussion is certainly not a presentation of research results on theoretical heat transfer, it is just an application of established theory to the design of heat exchangers for thermoacoustics.

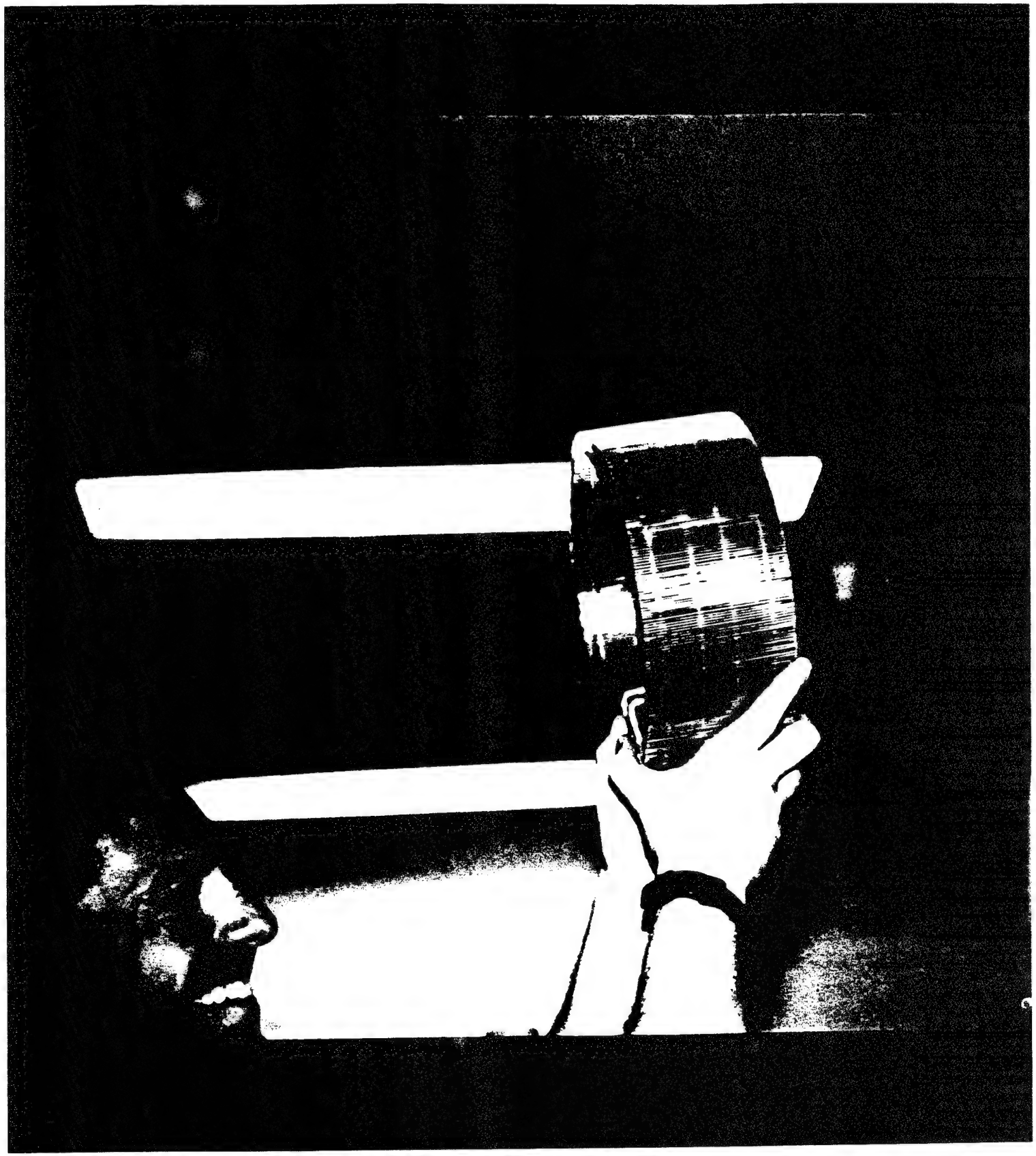

Figure 5. Heat exchanger for the radial wave prime mover.

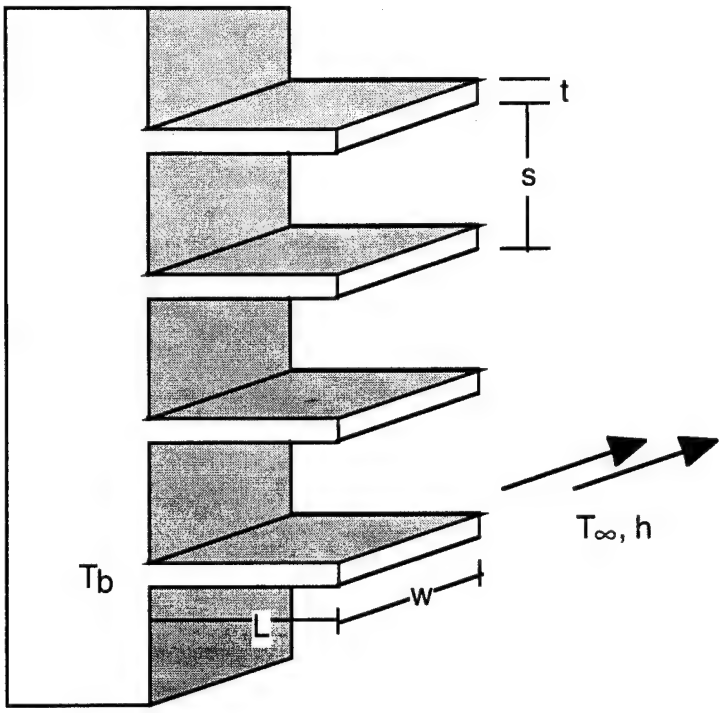

Figure 6. Heat exchanger schematic.

Figure 6 shows a heat exchanger schematic as it might be implemented in thermoacoustics. The base is at temperature T_b, and is a lower temperature than T_∞, the fluid temperature in the bulk of the fluid, so that heat may be removed from the fluid to the base. The length L can be considered the midway point between a base on the left and a similar base or fluid carrying tube (not shown) on the right. Fluid flows in the direction of the arrows, and the convective heat transfer coefficient is h. Ref. 6 quotes h to vary from 2-250 Watts/(m^2 K) for free and forced convection of gases, though due to the uncertainty of this factor, we will try to glean something about heat transfer without having to explicitly use h. Heat flux due to convection is parameterized as

$$q'' = (T_\infty - T_b)\, h \quad , \tag{2}$$

where q" is in units W/m^2.

In thermoacoustics, heat exchangers are usually pressed against the stack on one side and are open to the resonator on the other. Heat is transfered to the stack

from the heat exchanger by a number of processes. Heat is directly transfered by conduction from the stack solid material, through the stack and heat exchanger interface where contact resistance is an issue, and finally to the heat exchanger. Any convection of the gas in the stack also leads to heat transfer. Heat is also transfered by thermoacoustic action,[1] where we envision a parcel of gas at the heat exchanger and stack boundary making excursions both into the heat exchanger and a half cycle later into the stack. The gas is thought to transfer heat at the moment of greatest excursion when it is temporarily motionless. We might consider a strong acoustic wave with attendant high particle velocity as a source of convection as well when the gas is gushing through the heat exchanger on its way to its turn around point. Heat is also transferred between heat exchangers by black body radiation.

When used as a cold side heat exchanger for a refrigerator, the basic problem is that heat must be delivered from the heat exchanger at base temperature T_b to the gas at a lower temperature T_∞. Though the fins are shown terminating in Fig. 6, the termination should be viewed as the mid point between the base on the left and a base on the right. Gas will be considered to flow in a steady stream through the heat exchanger, and by Eq. (2), the heat transferred by convection will be locally dependent on the fin temperature. The ideal situation would be for the entire fin to be at the base temperature, for convection would then occur between temperatures T_b and T_∞. In this ideal case, the heat flow would

$$q_{max} = (T_\infty - T_b)\, h\, A_f \quad , \tag{3}$$

where A_f is the surface area of the fin. Making allowance for a temperature gradient along the fin, and assuming the fin tips are adiabatic, a fin efficiency for convection may be defined $\eta_f \equiv q_f/q_{max}$ where q_f is the actual heat transferred by convection, and from analysis,[6]

$$\eta_f = \frac{tanh\,(mL_c)}{mL_c} \quad , \tag{4}$$

where[6]

$$mL_c = \sqrt{\frac{2h}{k(L+t/2)\,t}}\ (L+t/2)^{3/2} \quad , \tag{5}$$

k is the fin thermal conductivity, L and t are given in Fig. 6, and h is the (unknown) convective coefficient. The leading correction for η_f is

$$\eta_f \approx \left(1 - \frac{4\,h\,L^2}{3\,kt}\right) \quad , \tag{6}$$

valid when $mL_c << 1$, or equivalently, $L << \sqrt{kt/h}$. Note that higher thermal conductivity and plate thickness t allow for longer heat exchanger sections between fluid filled tubes.

Equations (4) and (5) indicate that for high fin efficiency mL_c should be minimized, or put more bluntly, mL_c should be sent to 0. Eq. (5) indicates that to do this, the fin material should have as large a thermal conductivity as possible (no suprise there), that the fin length should be minimized (no suprise there either, since one can minimize a temperature for fixed temperature by shortening the span). It is somewhat suprising that Eq. (5) doesn't roll smoothly into a no fin solution when $L \rightarrow 0$, though there are some assumptions built into Eq. (5) that may obviate this limit. The greater the convective coefficient, the lesser the fin efficiency, since mL_c depends on the convective parameter h as the square root. This dependence on h is not anomalous, since with a higher convective parameter, more heat needs to be transferred. Finally, in the limit that $L >> t$, a usual limit in thermoacoustics, $mL_c \propto 1/\sqrt{t}$; hence it appears that a thicker fin is better than a thinner fin.

The actual heat transferred is given by

$$q_f = \eta_f\ h\ 2w(L+t/2)\ (T_b - T_\infty) \quad . \tag{7}$$

A commonly held view in thermoacoustics is that the plate width, w, should be about the same as the acoustic displacement amplitude. For an array of cooling fins, the overall fin efficiency is given by[6]

$$\eta_0 = 1 - \frac{2(L+t/2)}{2(L+t/2) + s} (1 - \eta_f) \quad . \tag{8}$$

For a fin array with plate spacing s << L (the usual case in thermoacoustics), the approximation $\eta_0 \approx \eta_f$ is good. Thus we can concern ourselves most with making η_f large for thermoacoustic considerations.

I have two problems with the foregoing convective theory. First, the coefficient h is not well known for our geometries. Its value probably lies between forced and free convection for gases. Second, all of the details of the temperature distribution between the plates has been swept into coefficient h. Another way of analyzing heat transfer in thermoacoustics is to compute the enthalpy flow at the left and right ends of a heat exchanger. By power conservation, any difference in these enthalpy values is to be attributed to power entering or exiting the heat exchanger as heat. Also, heat transferring by conduction from the stack, through the contact resistance, to the heat exchanger, contributes to the heat load at the exchanger. Is an appreciable amount of heat transferred by a classical steady breeze convective mechanism in thermoacoustics?

4. Publications.

a. W. P. Arnott, J. A. Lightfoot, R. Raspet, and H. Moosmüller, "Radial wave thermoacoustic engines: Theory and examples for refrigerators, prime movers, and high-gain narrow-bandwidth photoacoustic spectrometers," accepted for publication in J. Acoust. Soc. Am.

b. W. P. Arnott, H. Moosmüller, R. E. Abbott, and M. D. Ossosfsky, "Thermoacoustic enhancement of photoacoustic spectroscopy: Theory and measurements of the signal to noise ratio," submitted to Review of Scientific Instruments. (Numerical analysis developed within the ESSP program was used to aid in design of the thermoacoustic part of this research.)

c. J. A. Lightfoot, R. Raspet, H. E. Bass, and W. P. Arnott, "Thermoacoustic engines with varying plate separation," in preparation for J. Acoust. Soc. Am.

5. Other people associated with the project.

Two undergraduate Physics students from the University of Nevada are partially supported by this contract. They are seniors, and one of them (Michael Ossosfsky) has had extensive previous experience in the machine shop. The other student (Robert E. Abbott) is skilled at intricate parts manufacture. Together they work on a number of problems, such as constructing heat exchangers for the radial wave prime mover, and they also work on the thermoacoustic enhanced photoacoustic spectrometer project.

I am collaborating directly with the Ph.D. student Jay Lightfoot at the University of Mississippi. I visited the UM briefly during the contract period. Jay and I are modifying my thermoacoustic design numerical analysis program to evaluate general geometry engines. The Mississippi effort is directed by Dr. Richard Raspet.

6. References

1. G. W. Swift, "Thermoacoustic engines," J. Acoust. Soc. Am. **84**, 1145-1180 (1988).
2. W. P. Arnott, J. A. Lightfoot, R. Raspet, and H. Moosmüller, "Radial wave thermoacoustic engines: Theory and examples for refrigerators, prime movers, and high-gain narrow-bandwidth photoacoustic spectrometers," accepted for publication in J. Acoust. Soc. Am.
3. W. P. Arnott, H. E. Bass, and R. Raspet, "General formulation of thermoacoustics for stacks having arbitrarily shaped pore cross sections," J. Acoust. Soc. Am. **90**, 3228-3237 (1991).
4. J. A. Lightfoot, R. Raspet, H. E. Bass, and W. P. Arnott, "Thermoacoustic engines with varying plate separation," in preparation for J. Acoust. Soc. Am.
5. G. Bennett, "Active cooling for downhole instrumentation: a miniature thermoacoustic refrigerator," Dissertation, University of New Mexico (1991).
6. F. P. Incropera, and D. P. DeWitt, *Introduction to Heat Transfer*, (Wiley, New York, 1990).

APPENDIX 1
PREPRINT

Radial wave thermoacoustic engines: Theory and examples for refrigerators, prime movers, and high-gain narrow-bandwidth photoacoustic spectrometers

Radial wave thermoacoustic engines: Theory and examples for refrigerators, prime movers, and high-gain narrow-bandwidth photoacoustic spectrometers

W. Patrick Arnott[a)]
Atmospheric Science Center
Desert Research Institute
PO Box 60220
Reno, NV 89506

Jay A. Lightfoot, and Richard Raspet
Physics Department
University of Mississippi
University, MS 38677

Hans Moosmüller
Energy and Environmental Engineering Center
Desert Research Institute
PO Box 60220
Reno, NV 89506

(Received:

ABSTRACT

A theoretical analysis of radial thermoacoustic engines in cylindrical resonators is developed. Impedance and pressure translation equations are presented for open sections of the resonator and for heat exchangers. Coupled first order differential equations are given for pressure and impedance in the temperature gradient supporting engine section (stack). These quantities are used to calculate heat and work flows and to predict engine performance. Theory and design of a variable quality factor resonator for enhanced photoacoustic spectroscopy are presented. The short stack approximation is developed for the radial geometry and is used along with plane wave equations to compare refrigerator and prime mover performance for these two geometries. Results of the comparison are that engines in the plane wave geometry are better overall refrigerators when maximizing the coefficient of performance and cooling capacity together. Radial wave refrigerators are perhaps a better choice when cooling capacity is more important than coefficient of performance. The radial wave geometry yields prime movers with lower temperature gradients and higher efficiency for a given acoustic power load.

a) W. Patrick Arnott is an Adjunct Assistant Professor in the Department of Physics, University of Mississippi.

PACS #s 43.35.U, 43.28.F

1. LIST OF SYMBOLS

A_{res}	Cross sectional resonator area
a	resonator radius
C_m	coefficient of compromise
COP	coefficient of performance
COPc	Carnot coefficient of performance
c	sound speed
c_p	isobaric heat capacity per unit mass
d	thermoacoustic element length
F	thermoviscous dissipation function
f_0	resonance frequency
G	radial wave prime mover root function
$H_n^{(k)}$	Hankel function of order n and type k
h	resonator axial length
Im	imaginary part of
J_n	Bessel function of order n
k	complex propagation constant
k_0	adiabatic acoustics propagation constant
m	exponent for COP/COPc preference
N_{pr}	Prandtl number
P_0	ambient pressure
P_1	acoustic pressure
Q	quality factor of resonance
$\dot{Q}_2$	heat flow
R	twice pore or resonator cross sectional area divided by pore perimeter
r	radial coordinate
r_a, r_b	inner and outer radial stack radii. $r_b = r_a+d$
T_a, T_b	radial stack ambient temperatures at r_a, r_b
T_0	ambient temperature
T_1	acoustic i.e. excess temperature
T_{0r}	radial wave stack temperature gradient
$T_{0\infty}$	short stack radial wave temperature gradient
T_{0z}	plane wave stack temperature gradient
V_G	ambient volume of gas in the stack
v_s	standing wave particle velocity
$\dot{W}_2$	work flow
$\dot{W}_{ext}$	work flow external to the stack
$\dot{w}_{ext}$	dimensionless work flow external to the stack
Z	specific acoustic impedance
Z_{bl}	boundary layer specific acoustic impedance
Z_{int}	intrinsic impedance
z	axial coordinate
α	function used in stack impedance equation
β	coefficient of thermal expansion
γ	ratio, isobaric to isochoric specific heats
Γ	Swift's normalized temperature gradient
Δf	Photoacoustic spectrometer bandwidth
δ_κ	thermal penetration depth
ε	dummy variable
ε_s	Swift's plate heat capacity ratio
ϕ	normalized stack location
η	dynamic viscosity
η_r, η_p	radial and plane wave efficiencies, respectively
κ	thermal conductivity
λ	shear wave number = $\sqrt{2}\, R / \delta_\nu$
λ_T	Thermal disturbance number = $\sqrt{2}\, R / \delta_\kappa$
ρ_0	ambient gas density
ρ_1	acoustic gas density
τ	normalized stack temperature gradient
τ_{max}	refrigerator-stack normalized maximum temperature gradient
τ_{min}	prime mover stack normalized minimum temperature gradient
Ω	Stack or heat exchanger porosity
ω	radian frequency
ξ_s	standing wave particle displacement
ζ	stack or heat exchanger thickness
*	complex conjugation operator

I. INTRODUCTION

Thermoacoustic heat engines involve heat transfer between a solid and a fluid undergoing compression, expansion, and displacement. A comprehensive review is available[1] as is a review of the foundation work for modern thermoacoustics.[2] Most previous work considered placing thermoacoustic engines in plane wave resonators. A framework for analyzing and predicting the performance of engines in radial wave resonators is given in this paper.

Swift[1] briefly considered thermoacoustic engines in cylindrical resonators with only the lowest radial mode active. He developed the wave equation, discussed how to calculate energy flux, and showed a possible conceptual arrangement for a working engine. We advance upon Swift's work by establishing pressure and impedance translation equations for all points within the resonator. These equations are useful for computing acoustical quantities in open sections of the resonator, in heat exchangers, and in the temperature-gradient-supporting sections known as thermoacoustic engines. These relations naturally connect the various sections and give an explicit prescription for computing properties of complicated resonators containing several engines. This development parallels the previous analysis of engines in plane wave resonators.[3]

A conceptual design of a radial wave thermoacoustic engine is shown in Fig. 1. A cylindrical resonator is filled with a gas such as helium. The nominal pressure distribution is a radial or breathing mode. Thermoacoustic engines may be placed at either or both locations shown in Fig. 1 and are made of material with low thermal conductivity to support a temperature gradient. Since some of the first thermoacoustic engines were produced by stacking parallel plates, thermoacoustic engines are also referred to as stacks. The thermoacoustic elements are between pressure nodes and antinodes so that the product of acoustic pressure and particle velocity is significant. It is this product that is important for thermoacoustic transport of heat up the temperature gradient in the refrigerator application, or, in the sound source application, for producing net acoustic power when the applied temperature gradient is sufficiently large.[1-4] Heat exchangers made of material with high thermal conductivity are on both sides of the engine and are used to transfer heat between outside sources and sinks. Heat exchangers nearest the pressure antinodes are at higher temperatures than heat exchangers facing the pressure node. A full system would have many of the annuli shown in Fig. 1. The annuli would be stacked perpendicular to the plane of the figure with spacing between adjacent annuli of about one to two thermal penetration depths in the gas. The system can be operated as a sound source when high temperature gradients are applied across the engines, as a refrigerator when driven by an external acoustic source, or as a combination of both, just as with plane wave engines.[1]

Particle velocity and pressure distributions in empty resonators are of course different for radial and plane wave modes. For gas parcels in a standing wave, displacement and acoustic pressure are in phase which gives rise to a temperature gradient through the relation of pressure

and temperature. The temperature increase during compression of a gas parcel undergoing displacement in a standing wave is followed by a temperature decrease during expansion half a cycle later when the gas parcel is displaced in the opposite direction. This standing wave temperature gradient is useful to compare with temperature gradients applied to or developed on the stack.[1] For example in the inviscid limit where the Prandtl number N_{pr}=0, the stack will operate as a refrigerator when its temperature gradient is less than the standing wave gradient and as a prime mover when its temperature gradient is larger than the standing wave gradient. The temperature gradient associated with standing waves in empty plane and radial resonators are considered to gain familiarity with some differences between plane and radial wave geometries . Swift[1] refers to this as the critical mean-temperature gradient, ∇T_{crit}. The coordinate system and possible stack locations for radial and plane engines are shown schematically in Figs. 2a and 2b. The critical temperature gradients are

$$\frac{h\beta\, T_{0z,c}}{\gamma - 1} = -\pi\, \frac{cos\,(\pi z/h)}{sin\,(\pi z/h)} \qquad , \qquad \frac{a\beta\, T_{0r,c}}{\gamma - 1} = -3.832\, \frac{J_0\,(3.832 r/a)}{J_1\,(3.832 r/a)} \qquad (1a,b)$$

where $T_{0z,c}$ and $T_{0r,c}$ are the critical mean-temperature gradients associated with plane and radial waves, respectively.

Figure 3 shows the critical temperature gradients. In the inviscid approximation, engines act as refrigerators when the ambient temperature gradient on the stack is in the region between the curves and zero temperature gradient line; otherwise, engines are prime movers (sound sources). The curves cross this line at pressure nodes. The pressure node for the radial case occurs at r/a≈0.63. Some qualitative conclusions are that radial refrigerators with stacks between $0 < r/a < 0.63$ can achieve larger temperature gradients than plane wave refrigerators, and that radial prime movers with stacks between $0.63 < r/a < 1$ will operate at lower temperature gradients than either plane wave prime movers or the other radial prime mover. The latter of these conclusions is not true when gas viscosity is included as will be shown below.

This paper is organized as follows. Section II and its subsections contain the formal solution for the first order acoustic properties of pressure, specific acoustic impedance, and the second order enthalpy flow. Section IIC is an application of the general theory which serves the dual purpose of teaching the calculation techniques and of demonstrating an interesting dependence of resonance frequency on stack plate spacing. The application has relevance to design of thermoacoustically enhanced photoacoustic spectrometers.[5] The short stack approximation similar to that given for plane waves[3] (not limited by the additional boundary layer approximation[1]) is presented in Sec. III, and is used in its subsections to compare the performance of plane and radial wave refrigerators and prime movers.

II. RADIAL WAVE ANALYSIS

A system of equations is established for computing pressure, specific acoustic impedance, and enthalpy flow at all points. Enthalpy flow can be evaluated when pressure and impedance are known, and is needed for estimation of the engine efficiency and power. The analysis closely parallels that given for plane wave systems[3] and for that reason the treatment here is brief.

Figures 2a and 2b show the coordinate system. Analysis proceeds by breaking the engine up into the three types of regions, shown schematically in Fig. 1, for the purpose of isolating elements that can be evaluated by the same type of equations and that have similar acoustic properties. Region 1 contains the resonator center where, by symmetry, a pressure antinode and particle velocity node exist. Region 2 is the thermoacoustic engine and will also interchangeably be referred to as the stack in this paper. The stack usually has a radial temperature gradient. Region 3 is associated with resonator and heat exchanger sections. Specific acoustic impedance and pressure translation theorems are derived for analyzing wave propagation in region 3 thermoacoustic elements. These equations are analogous to Rayleigh's impedance translation theorem for plane waves.[3,6] Analyses for electromagnetic waves in radially symmetric layered media,[7] and of radial acoustic waves in ducts with finite impedance walls,[8] have features similar to the approach taken here in the analysis of regions 1 and 3.

The basic set of equations used by Rott[2] for analyzing plane wave engines can be altered for use in analyzing radial wave engines.[1] The $exp(-i\omega t)$ convention is used. All components of particle velocity and the excess temperature, T_1, are taken to be zero at the fluid-solid boundary. The excess temperature boundary condition is appropriate when the product of stack density, heat capacity per unit mass, and thermal conductivity is much greater than the same product for the working fluid, and when the stack plate thickness is much greater than the thermal penetration depth in the solid material of the stack.[1] Both criteria for using the zero excess temperature boundary condition are usually satisfied in practice when the working fluid is a gas at moderate pressure. This boundary condition is the $\varepsilon_s \rightarrow 0$ limit of the equations in Ref. 1.

A. Specific acoustic impedance and pressure translation theorems, and enthalpy flow.

Counterpropagating radial waves having different complex amplitudes may be superimposed to describe wave propagation in open resonator and heat exchanger sections. Boundary conditions at interfaces are continuity of acoustic pressure and continuity of specific acoustic impedance. However, in the stack sections where the ambient temperature depends on position, coupled first order differential equations are used to determine acoustic pressure, specific acoustic impedance, and in some instances the ambient temperature.

Denote by Z(r) the specific acoustic impedance at position r. Z(r) is the acoustic pressure divided by the volume of gas passing through r per unit area per unit time. The intrinsic or characteristic impedance of a section of resonator, heat exchanger, or stack is given by

$$Z_{int} = \frac{\rho_0 \omega}{\Omega F(\lambda) k} \quad , \tag{2}$$

where $\Omega = R/(\zeta + R)$ is the porosity, R is the plate spacing, and ζ is plate thickness. The thermoviscous dissipation function for the parallel plate geometry is[1,3,9]

$$F(\varepsilon) = 1 - \frac{2}{\varepsilon\sqrt{-i}} \tanh\left(\frac{\varepsilon\sqrt{-i}}{2}\right) . \tag{3}$$

The dummy variable $\varepsilon=\lambda_T$ when thermal dissipation is considered, and $\varepsilon=\lambda$ for viscous dissipation. Other parameters are the Prandtl number $N_{pr} = \eta c_p/\kappa$, the dimensionless shear wave number $\lambda = (\rho_0 \omega/\eta)^{1/2} R$ and thermal disturbance number $\lambda_T = \lambda N_{pr}^{1/2}$. The quantity R when computing Eq. (3) is the spacing between heat exchanger annuli, or the distance between the top and bottom plates (h in Fig. 2a) for open sections of the resonator. The complex propagation number k is given by

$$k^2 = \frac{\omega^2}{c^2} \frac{\gamma - (\gamma - 1)F(\lambda_T)}{F(\lambda)} \quad , \tag{4}$$

where c is the adiabatic sound speed.

Determined first are the acoustic pressure and specific acoustic impedance in the resonator and heat exchanger sections shown as region 3 in Fig. 1. These quantities at position r-d can be determined through use of pressure and impedance translation equations which use given values of these quantities at position r. Using a procedure similar to that outlined in Ref. 3, the translation equation for pressure is

$$P_1(r-d) = P_1(r) \frac{\pi k r i}{4} \left\{ H_1^{(1)}[kr]\, H_0^{(2)}[k(r-d)] - H_1^{(2)}[kr]\, H_0^{(1)}[k(r-d)] \right.$$
$$\left. - i \frac{Z_{int}}{Z(r)} \left(H_0^{(2)}[kr]\, H_0^{(1)}[k(r-d)] - H_0^{(1)}[kr]\, H_0^{(2)}[k(r-d)] \right) \right\} . \tag{5}$$

The translation equation for specific acoustic impedance is

$$Z(r-d) = Z_{int} \left\{ Z(r) \left(H_1^{(1)}[kr]\, H_0^{(2)}[k(r-d)] - H_1^{(2)}[kr]\, H_0^{(1)}[k(r-d)] \right) \right.$$
$$\left. - i\, Z_{int} \left(H_0^{(2)}[kr]\, H_0^{(1)}[k(r-d)] - H_0^{(1)}[kr]\, H_0^{(2)}[k(r-d)] \right) \right\} /$$
$$\left\{ Z_{int} \left(H_1^{(1)}[k(r-d)]\, H_0^{(2)}[kr] - H_1^{(2)}[k(r-d)]\, H_0^{(1)}[kr] \right) \right.$$
$$\left. - i\, Z(r) \left(H_1^{(1)}[k(r-d)]\, H_1^{(2)}[kr] - H_1^{(2)}[k(r-d)]\, H_1^{(1)}[kr] \right) \right\} . \tag{6}$$

Hankel functions $H_m^{(j)}[x]$ of order m, type j, and argument x are used in Eqs. (5) and (6). It can be shown using the asymptotic expansion for Hankel functions with $x >> 1$, $H_n^{(1)}(x) \approx (2/\pi x)^{1/2} \exp\ [i\,(x - n\pi/2 - \pi/4)]$ and $H_n^{(2)}(x) \approx (2/\pi x)^{1/2} \exp\ [-i\,(x - n\pi/2 - \pi/4)]$, that Eqs. (5) and (6) reduce to the one dimensional plane wave forms given in Ref. 3.

Specific acoustic impedance and acoustic pressure are determined in the stack, region 2 in Fig. 1, as follows:

$$\frac{dZ(r)}{dr} = i\,k(r)\,Z_{int}(r)\left(1-\frac{Z(r)^2}{Z_{int}(r)^2}\right) + \left(2\,\alpha(r)+\frac{1}{r}\right)Z(r)\,, \tag{7}$$

and

$$\frac{dP_1(r)}{dr} = i\,k(r)\,Z_{int}(r)\,\frac{P_1(r)}{Z(r)}\quad, \tag{8}$$

where $\alpha(r)$ is given by

$$\alpha = \frac{\beta\,T_{0r}}{2}\,\frac{F(\lambda_T)/F(\lambda) - 1}{1 - N_{pr}}\quad. \tag{9}$$

The temperature gradient along the plate in the radial direction is given by $T_{0r} = dT_0(r)/dr$. All parameters such as α and k are dependent on r since the ambient temperature generally depends on r in the stack. Except for the term involving 1/r in Eq. (7), Eqs. (7-8) are the same as their plane wave counterparts given in Ref. 3.

The expressions for heat, work, and enthalpy flows for the radial wave geometry are the same as the plane wave geometry equations.[1] Expressions for heat, and work flows are given in terms of acoustic pressure and specific acoustic impedance in Ref. 3. For the radial wave geometry, it is important to note the dependence of enthalpy flow on the cross sectional area of the resonator as $A_{res}(r) = 2\pi rh$. By contrast, the plane wave geometry has $A_{res} = \pi a^2$.

B. Numerical implementation of the theory.

Recent theoretical and experimental work has considered the effect of stack temperature gradient on the resonator quality factor Q, and resonance frequency f_0.[4,10-13] The quantity 1/Q is the dissipated acoustic power per radian frequency per stored acoustic energy throughout the entire resonator. Although acoustic power is normally absorbed through the processes of heat conduction and viscous dissipation at interfaces between solids and fluids, a stack with an appropriate temperature gradient can generate acoustic power.[4,12] Resonance frequency is determined by thermoacoustic element lengths and dispersion caused by narrow plate spacing. Both Q and f_0 can be incorporated into a single quantity, the complex eigenfrequency $\omega_c = 2\pi f_0 - i\pi f_0/Q$, which describes the temporal response throughout the resonator of an excited resonance at t=0, $P_1(t)/P_1(0) = exp\ (-i\omega_c t)$. The complex eigenfrequency of a radial wave prime mover below the onset of self oscillation will be computed to illustrate the appropriate technique for the radial geometry, and to point out the dependence of f_0 on stack plate spacing.

When determining the quality factor or onset temperature for plane wave systems, it is usually sufficient to consider a constant temperature gradient in the stack.[4,12] For the radial geometry, however, because a constant amount of heat is spread into an increasing area as r increases, the ambient temperature gradient is given by

$$T_{0r}(r) = T_{0\infty}\,\frac{d}{r}\,\frac{1}{ln\,(1 + d/r_a)}\,, \tag{10}$$

where $d=(r_b - r_a)$ is the stack length, r_a and r_b are the inner and outer radius of the stack, and $T_{0\infty}=(T_b - T_a)/(r_b - r_a)$. Note that $T_{0r}(r) \approx T_{0\infty}$ when $d << r_a$ as is the case in the short stack approximation below, and when $r_a \rightarrow \infty$ which approximates the plane geometry.

The complex eigenfrequency can be determined by numerically searching for values of f_0 and Q that give the same result for the calculated impedance looking to the right at some position, with that computed looking to the left.[4] Consider the resonator region 1 in Fig. 1. By symmetry, a particle velocity node must occur at the resonator center, yielding an expression for the acoustic pressure,

$$P_1(r) = P_1(0)\, J_0\,(kr) \quad , \tag{11}$$

and for the specific acoustic impedance,

$$Z(r) = -i\, Z_{int} \frac{J_0\,(kr)}{J_1\,(kr)} \quad . \tag{12}$$

Equations (11) and (12) can be obtained by using $r \rightarrow 0$, $d \rightarrow -r$, and $Z(0) \rightarrow \infty$ in Eqs. (5) and (6), respectively, so region 1 in Fig. 1 can be regarded as a special case of region 3. The complex propagation number k is from Eq. (4), and the intrinsic or characteristic impedance is from Eq. (2) with $\Omega=1$. Note that even though $i = \sqrt{-1}$ occurs in Eq. (12), impedance is not purely imaginary because of the complex propagation number k. In other words, Z(r) in region 1 must still reflect the fact that thermal and viscous dissipation occurs at the resonator walls. Define Z_- as the specific acoustic impedance at the inside boundary of the heat exchanger that faces the resonator center. Z_- is computed from Eq. (12) using the appropriate inner radius of this heat exchanger. It is now necessary to substitute the complex eigenfrequency ω_c for ω in Eqs. (5)-(6) and Eq. (12).

Z_- is stored as the impedance looking towards the resonator center from the inner radius of the heat exchanger. Eventually Z_- must be compared with Z_+, where Z_+ is the impedance at the same location, but looking towards the resonator wall. To compute Z_+, begin at the resonator wall where impedance is much greater than the characteristic impedance $\rho_0 c$, but is finite because thermal dissipation occurs during the acoustic cycle as the gas undergoing compression and expansion exchanges heat with the wall. The boundary layer impedance, denoted by Z_{bl}, for the cylinder wall can be shown to be[14]

$$Z_{bl} = -\frac{\rho_0 c^2}{\gamma - 1} \sqrt{\frac{\rho_0 c_p}{i\omega\kappa}} \frac{J_0\,[(1+i)a/\delta_\kappa]}{J_1\,[(1+i)a/\delta_\kappa]} \approx \frac{\rho_0 c^2}{\gamma - 1} \sqrt{\frac{i\rho_0 c_p}{\omega\kappa}} \qquad \text{for } a >> \delta_\kappa \ . \tag{13}$$

In Eq. (13) $\delta_\kappa = \sqrt{2\kappa/\rho_0\omega c_p}$ is the thermal boundary layer thickness (ie. the distance heat can diffuse during time $1/\omega$), and the second approximate form is just the expression for boundary layer impedance when the wall is flat.[6,14] In thermoacoustics the second form of Z_{bl} is applicable since $a >> \delta_\kappa$.

Having established Z_{bl}, impedance at the outer radius of the outer heat exchanger is computed using Z_{bl} and Eq. (6). This value of impedance is used again with Eq. (6) to compute impedance at the outer radius of the stack (region 2 in Fig. 1), though this time with k and Z_{int} appropriate for the heat exchanger and with d the heat exchanger length. Using Eq. (7) and our computed impedance at the outer stack border as the boundary condition, numerical integration of the differential equation yields the impedance at the inner stack border. Finally, Eq. (6) is used again to translate impedance from the inner stack boundary to the inner boundary of the inner heat exchanger. Denote this value of impedance as Z_+. If it is found that $Z_- = Z_+$, then our current choice of ω_c is the complex eigenfrequency; otherwise, the entire procedure must be repeated with another trial value of ω_c. Note that both the real and imaginary parts of impedance must be matched by adjusting both the real and imaginary parts of ω_c, which is equivalent to adjusting f_0 and Q.

It should be noted that this procedure can be used to compute $Q<0$ (i.e. exponential increase rather than decrease of acoustic pressure in the resonator) that occurs for a superheated prime mover for a short time after Q spoiling ceases.[13] When a prime mover goes into onset, the resonator has become unstable with respect to acoustic oscillations, and $Q \rightarrow \infty$. The eigenfrequency is real in this case and is given simply by $\omega_c = 2\pi f_0$. Stability curves for the prime mover[4,11] can be computed by adjusting values of f_0 and $T_{0\infty}$ until impedance is matched. Different resonator modes can be studied by choosing appropriate starting values of f_0.

C. Design of a thermoacoustic enhanced photoacoustic spectrometer.

The example calculation for resonance frequency and Q of a radial prime mover considers the outer stack location. Specific dimensions will be used in describing the resonator, heat exchangers and stack. Resonator overall dimensions are similar to those reported in photoacoustic spectroscopy measurements performed using empty resonators[15,16] (no thermoacoustic elements). Refer to Fig. 4. A laser beam modulated at the acoustic resonance frequency passes through the resonator to couple energy into a particular resonator mode when light is absorbed by aerosols and/or particular gaseous species.[15,16] The acoustic signal is proportional, among others, to the laser power, to the absorption coefficient of the gaseous species or aerosol (hence the connection with spectroscopy), and to the resonator Q. Thermoacoustics offers the possibility of adjusting Q by controlling the temperature gradient of the stack. Resonator Q increases with the applied temperature gradient when the hot end of the stack faces a pressure antinode and decreases when the hot end faces a pressure node. It can be shown that when the acoustic noise in the resonator is Gaussian, and when the bandwidth of the microphone detection electronics is much greater than the resonator bandwidth, the signal to noise ratio for the measurement scales as $Q^{1/2}$. The $Q^{1/2}$ dependence of the signal to noise ratio can be qualitatively understood as follows: signal and noise are both enhanced by Q; however,

the noise bandwidth is proportional to $Q^{-1/2}$. Hence it is desirable to perform photoacoustic spectroscopy with high Q resonators. A thermoacoustic enhanced resonator can be described as an analog amplifier with adjustable gain Q for frequency f_0, with adjustable bandwidth $\Delta f=f_0/Q$, and with discrimination of signal against acoustic Gaussian noise of $Q^{1/2}$.

Refer to Fig. 4. System dimensions are specified starting at resonator center. The inner portion of the resonator, the ambient heat exchanger, and the inner radius of the stack all are assumed to be at an ambient temperature T_a = 293 K. The quantity $T_{0\infty}$ in Eq. (10) will be held at a constant value $T_{0\infty}$ = 26.6 K/mm. The resonator height is taken as h = 5 cm. The distance from resonator center to the ambient heat exchanger is 8.98 cm. The cold heat exchanger is 1.08 mm long. Three stack lengths are considered: d = 3.28 mm, 0.8d, and 1.2d. The quantity R denotes both the stack and heat exchangers plate spacings, and will vary in the calculation. The plates thus become thicker as R increases since the calculation is for constant stack and heat exchanger porosity Ω=0.7. The hot heat exchanger is 1.15 mm long. The section from the hot heat exchanger to the outer diameter of the resonator is 9.98 mm long, and its temperature is T_b=380.2 K for d=3.28mm, is T_b=362.8 K for 0.8d, and is T_b=397.7 K for 1.2d. The working fluid is taken as dry air with ambient pressure P_0 = 100 kPa. For comparative purposes the resonance frequency and Q were computed for both an empty resonator having diameter 21.06 cm, and for the above thermoacoustic arrangement when $T_{0r}(r) = 0$.

Figures 5a) and 5b) show the resonance frequency, f_0, and Q as a function of stack and heat exchanger plate spacing, R. The empty resonator has $f_0 \approx 1984$ Hz and $Q \approx 550$. The case of no stack temperature gradient and Fig. 5a) will be considered first. Starting at largest R, f_0 decreases as R decreases because the phase velocity in stack and heat exchangers also decreases. Now as $R \rightarrow 0$, f_0 increases since the attenuation of sound in the stack and heat exchangers is quite severe, and the characteristic impedance of these elements $\rightarrow \infty$. Hence the cold heat exchanger begins to approximate a nearly rigid termination and f_0 is approximately determined using the distance from the resonator center to the cold heat exchanger and the ambient sound speed. The minimum f_0 occurs as a trade-off of these dependencies on R. In Fig. 5b) Q increases with R for no temperature gradient because the thermal and viscous boundary layers become smaller in relation to the plate spacing so the attendant losses decrease. Note that Q also increases as $R \rightarrow 0$ because the cold heat exchanger better approximates a rigid termination in this limit.

A fundamentally different dependence for Q occurs when the stack has a sufficiently large temperature gradient. Q increases by as much as a factor of 2 over the empty resonator value for a stack plate spacing of $R \approx 0.21$ mm. The thermal disturbance number at the hot end corresponding to this value of R and the stack with length 1.2 d is $\lambda_T \approx 3.81$, which gives $R/\delta_\kappa \approx 2.7$. Gas within $\approx 1.35\ \delta_\kappa$ of the stack walls receives some acoustic power gain due to the

temperature gradient in addition to the normal viscous and thermal losses present with no temperature gradient.[4] This result again[1–4] demonstrates that the important length scale for optimal thermoacoustic performance is δ_κ. The stack is longest for the thickest line in Figs. 5a) and 5b), which produces the greatest thermoacoustic gain (i.e. highest Q) since, as shown in the short stack approximation below, acoustic power production and dissipation in the stack are proportional to stack length. As R increases beyond the value for maximal Q, the volume of gas receiving thermoacoustic gain decreases as does Q. For $R \rightarrow 0$, Q decreases since the gas begins to take on the same temperature as the stack (thermoacoustic drive ceases) and viscous losses increase.

The bending-up of the resonance frequency curves in Fig. 5a) for decreasing $\lambda_T=R/\delta_\kappa$ has previously been observed experimentally for a stack in a plane wave resonator where the ambient gas pressure and hence δ_κ was varied, though no explanation of the effect was given.[4] Note that the frequency bends up for larger plate spacing as the hot end temperature increases. This can be explained in part by noting that $\delta_\kappa \propto (\kappa/\rho_0)^{1/2}$ increases with increasing temperature. Hence as the hot end temperature increases, λ_T decreases and the resonance frequency can bend up for larger R than when no stack temperature gradient is present.

Close examination of Fig. 5a-5b shows that the peak in Q for a particular plate spacing occurs in the vicinity of rapid variation of the resonance frequency. It is unfortunate that the peak in Q does not correspond to the relative minimum of resonance frequency. If it did, slight variations in any of the parameters, such as ambient temperature and pressure, would cause only small changes of the resonance frequency. It should be noted that a similar dependence for Q and resonance frequency were obtained for the plane wave geometry, and that this geometry can also be used to increase the Q of these resonators for photoacoustic spectroscopy.

III SHORT STACK APPROXIMATION

The short stack approximation[1,3,4] is given and used to compare some basic properties of radial and plane wave engines. Basic assumptions are discussed in Refs. 1,3, and 4. The stack temperature gradient is the constant $T_{0\infty}$ in the short stack approximation (see the discussion below Eq. (10)).

Pressure, particle velocity, and particle displacement amplitudes between the stack end and the resonator wall are taken to be the standing wave forms

$$P_1(r) = P_1(0)\, J_0(k_0 r) \quad , \qquad P_1(z) = P_1(0)\, cos\,(k_0 z) \quad , \tag{14a,b}$$

$$v_s(r) = \frac{P_1(0)}{\Omega \rho_0 c}\, J_1(k_0 r) \quad , \qquad v_s(z) = \frac{P_1(0)}{\Omega \rho_0 c}\, sin\,(k_0 z) \quad , \tag{15a,b}$$

$$\xi_s(\phi) = \frac{v_s(\phi)}{\omega} \quad , \tag{16}$$

where Eqs. (14a) and (15a) [Eqs. (14b) and (15b)] refer to the radial [plane] wave geometry. The wavenumber in the empty tube is $k_0=\omega_0/c$ and ω_0 is the resonance radian frequency, Ω is stack porosity, and ϕ refers to either phase k_0r or k_0z. Use of Eqs. (14-16) in Eq. (50) of Ref. 3 readily yields

$$\bar{Q}_2(\phi) = -\frac{\Omega A_{res}\, P_1(\phi)\, v_s(\phi)}{2}\,\beta T_0\,\frac{Im\,[F^*(\lambda_T)F^*(\lambda)]}{(1+N_{pr})\,|F(\lambda)|^2}$$
$$-\frac{\rho_0\, c_p\, \Omega A_{res}\, v_s(\phi)}{2}\,\frac{Im\,\{F^*(\lambda_T)+N_{pr}\,F(\lambda)\}}{(1-N_{pr}^2)\,|F(\lambda)|^2}\,\xi_s(\phi)\;T_{0\phi}\;. \qquad (17)$$

where $T_{0\phi} = T_{0r}$ and $T_{0\phi} = T_{0z}$ are the constant temperature gradient for radial and plane wave geometry, respectively. The first term in Eq. (17) is the time averaged heat flow due to compression of the gas and can be exploited to construct acoustic refrigerators.[1] This heat flows in the stack towards the nearest pressure antinode, and thus heat is transported from the cold to the hot end of the stack. Gas displaced to a region with different stack wall temperature results in heat transfer given by the second term of Eq. (17).[1] This heat always flows from the hot to cold end of the stack and is independent of β. The stack acts as a refrigerator when the magnitude of the first term is larger than the magnitude of the second and the signs of these two terms are different. The second term of Eq. (17) thus reduces the cooling capacity of the refrigerator. For a prime mover, the magnitude of the second term in Eq. (17) is greater than the magnitude of the first term, so net heat is transported from hot to cold.

The work done in the stack is computed by use of the impedance translation theorem .[3] Denote by $V_G = A_{res}\,\Omega\, d$ the ambient volume of gas in the stack. The work flow to first order in k_0d can be shown to have the same form as for the plane wave geometry,[3,4,17]

$$\bar{W}_2(\phi) = \omega\,\frac{V_G\,P_1^2(\phi)}{2\,\rho_0\,c^2}\,(\gamma-1)\,Im\,F^*(\lambda_T) + \omega\,\frac{\rho_0\,V_G\,v_s^2(\phi)}{2}\,\frac{Im\,F^*(\lambda)}{|F(\lambda)|^2}$$
$$+\frac{V_G\,P_1(\phi)\,v_s(\phi)}{2}\,\beta\,T_{0\phi}\,\frac{Im\{F^*(\lambda_T)/F^*(\lambda)\}}{1-N_{pr}}\;. \qquad (18)$$

The first and second terms, always > 0, are dissipation of potential and kinetic energy per unit time due to thermal and viscous effects. The third term is acoustic power produced or absorbed by the stack due to the ambient temperature gradient, and makes possible use of a thermoacoustic engine as a sound source. The stack will produce sound when the last term has a sign different than the first two terms, and a magnitude greater than the sum of these terms.

The resonator area at the stack is $A_{res}=2\pi rh$ [$A_{res}=\pi a^2$] for radial [plane] wave geometry . Referring to Eq. (18), potential energy dissipation is proportional to $\{A_{res}\,P_1^2(\phi)\}$, kinetic energy dissipation is proportional to $\{A_{res}\,v_s^2(\phi)\}$, while thermoacoustic gain is proportional to $\{A_{res}$

$P_1(\phi)v_s(\phi)\}$. These quantities are shown in Fig. 6a for plane, and Fig. 6b for radial geometry. Note the high symmetry in Fig. 6a, and lack thereof in Fig. 6b for the radial geometry. Referring to Figs. 2a-b and Figs. 6a-b, one would like to place the stack at the locations of maxima for thermoacoustic gain; however, KE loss (which is usually more severe than PE loss) can be significantly reduced by placing the stack closer to pressure antinodes at the price of a slightly smaller thermoacoustic gain. Gain and losses $\rightarrow 0$ as $r \rightarrow 0$ for the radial geometry in Fig. 6b due to the dependence on A_{res}.

A number of assumptions are necessary to compare radial and plane geometry refrigerators and prime movers. The assumptions common to both refrigerators and prime movers are given here. The same resonator will be used for both geometries in the comparison though the stack configuration will be as shown in Fig 2a (Fig. 2b) for the radial (plane) geometry. Resonator aspect ratio a/h is determined by the condition that plane and radial stacks operate in resonators with the same eigenfrequency (a condition likely to be avoided in practice). The conditions for determining plane and radial propagation numbers are $k_0h = \pi$ and $k_0a=3.832$. Thus the resonator aspect ratio is $a/h=3.832/\pi$. The working fluids are Helium or a mixture of 60% Helium and 40% Argon so the assumed Prandtl numbers are $N_{pr} = 2/3$ or $N_{pr} = 0.392$, respectively. Ideal gas relations are used for other gas properties such as coefficient of thermal expansion and ratio of specific heats. The dimensionless thermal disturbance number $\lambda_T = (\rho_0 c_p \omega/\kappa)^{1/2} R = \sqrt{2}\, R/\delta_\kappa$, is used to characterize the dynamic thermal interaction between fluid and solid, where R is the stack plate spacing. The maximum potential energy density[1] (which is half the stored overall energy density) in each resonator is assumed to be equal in both cases, and is used to normalize the acoustic pressure using the relation $(1/V)\int P_1(\phi)^2 dV = 1$. Here V is the resonator volume, and it is assumed that even when a short stack is present the pressure relations, Eqs. (14a,b), are valid throughout the resonator. The normalization of radial (plane) geometry is $P_1(0) = 2.483$ $(\sqrt{2})$.

A nondimensional temperature gradient was previously[4] helpful in the analysis of prime mover performance, and will also be used here. It is given by

$$\tau \equiv \frac{\beta \Delta T_0}{2 k_0 d} \tag{19}$$

where d is the stack length, $\Delta T_0 = (d\, T_{0\infty})$ for radial and $\Delta T_0 = (d\, T_{0z})$ for plane geometries [see the discussion below Eq. (10)] is the ambient temperature difference between stack ends and can be positive or negative. The stack location is specified by the phase $\phi(r)=k_0r$ $[\phi(z)=k_0z]$ for radial [plane] geometry. By combining the expression for A_{res} with the expressions above defining the resonator dimensions, $k_0^2 A_{res}=2\pi^2\phi(r)$ $[k_0^2 A_{res}=3.832^2\, \pi]$ for radial [plane] geometry. The dimensionless forms of plate spacing λ_T, stack location ϕ, and stack temperature gradient τ are an example of similitude as applied in thermoacoustics.[18]

A. Comparison of radial and plane wave refrigerators.

Refrigerators, cryocoolers, and air conditioners are usually designed for a given cooling temperature and cooling capacity. The Coefficient of Performance, COP, is the ratio of cooling capacity to the input power necessary to operate the refrigerator , and is usually also specified as a design criteria. The Carnot COP will be denoted as COPc and is the highest COP possible for a given temperature span.[1] A refrigerator designed solely for high cooling capacity will likely have low COP, so often a trade-off between high cooling capacity and high COP must be accepted. Some design choices for thermoacoustic refrigerators are the working fluid and its ambient pressure, resonator size, sound source, heat exchangers capacity, stack geometry and material of construction, stack length and its location in the standing wave, and resonator mode (plane or radial) to use. With such a large list of design criteria and possible design configurations to consider, the challenge of comparing radial and plane wave geometry thermoacoustic heat pumps appears at first to be daunting. Granted, no single set of criteria covers all aspects of refrigerator design. However some design exploration using a reasonable set of system equations helps to build our intuition.

As an aid for determining how to compare radial and plane wave acoustic refrigerators, consider the simple example developed by Swift[1] for his purpose of illuminating basic acoustic refrigerator properties. The example assumes an inviscid gas ($N_{pr} = 0$) and the boundary layer approximation for the thermal interaction of gas and stack. Heat flow in this example (using our notation) is $\dot{\bar{Q}}_2(\phi) = -(A_{res}/\sqrt{2}\lambda_T)\,\beta T_0\,P_1(\phi)\,v_s(\phi)\,(1 - \Gamma)$ where $\Gamma = T_{0\phi}/T_{0\phi,c}$ is the ratio of the actual stack temperature gradient to the critical temperature gradient given in Eqs. (1a-b) for plane and radial geometries. Coefficient of Performance is $COP = \Gamma COPc$. For refrigerators, $0 < \Gamma < 1$. Immediately appreciate that to increase COP/COPc, $\Gamma \approx 1$ is desirable. However, the cooling capacity of the refrigerator $\dot{\bar{Q}}_2(\phi) \to 0$ as $\Gamma \to 1$. An acoustic refrigerator with large COP is likely to have low cooling capacity.

Our purpose here is to compare radial and plane wave refrigerators, not, for example, to decide on the best working fluid. To this end a useful quantity, the Coefficient of Compromise C_m, is defined as

$$C_m \equiv \left(\frac{COP}{COPc} \right)^m \left| \dot{\bar{Q}}_2(\phi) \right| \quad , \quad (m \geq 0) \tag{20}$$

where different values of m can be used to choose a desired compromise between COP and cooling capacity. For example, C_1 refers to refrigerator design where Coefficient of Performance and cooling capacity are similarly emphasized, and C_5 has Coefficient of Performance emphasized considerably more than cooling capacity. C_m has units of Watts. The next task is to show how to calculate C_m for radial and plane wave refrigerators to within a common factor.

The Coefficient of Performance is $COP=\bar{\dot{Q}}_2(\phi)/\bar{\dot{W}}_2(\phi)$. A technique similar to Swift's[1] is used to obtain $COPc=T_C/\Delta T_0$ where T_C is the stack cold end temperature and $\Delta T_0=(T_H-T_C)$ is the temperature difference of the stack ends. Using the definition of τ in Eq. (19), the thermodynamic identity $\beta^2 T_0 c^2=(\gamma - 1)/c_p$, and Eqs. (17)-(18) for heat and work flows, gives

$$\frac{COP}{COPc} = \frac{-2\tau\left(\frac{J_0(\phi)J_1(\phi)}{\Omega} \frac{Im\,[F^*(\lambda_T)F^*(\lambda)]}{(1+N_{pr})\,|F(\lambda)|^2} + \frac{2J_1^{\,2}(\phi)}{\Omega^2} \frac{1}{\gamma-1} \tau \frac{Im\{F^*(\lambda_T)+N_{pr}\,F(\lambda)\}}{(1-N_{pr}^2)\,|F(\lambda)|^2} \right)}{(\gamma-1)J_0^{\,2}(\phi)Im\,F^*(\lambda_T) + \frac{J_1^{\,2}(\phi)}{\Omega^2} \frac{Im\,F^*(\lambda)}{|F(\lambda)|^2} + 2\tau \frac{J_0(\phi)J_1(\phi)}{\Omega} \frac{Im\,\{F^*(\lambda_T)/F^*(\lambda)\}}{1-N_{pr}}} \qquad (21)$$

for radial wave refrigerators. The plane wave refrigerator COP/COPc is also given by Eq. (21) with the replacements $J_0(\phi)\rightarrow cos(\phi)$ and $J_1(\phi)\rightarrow sin(\phi)$. The stack length, d, can be calculated using $k_0 d=(\beta T_0)/(2|\tau|\,COPc)$.

Heat flow $\bar{\dot{Q}}_2(\phi)$ is given in a different form from Eq. (17) to show how it is calculated in Eq. (20) to obtain C_m. The rewritten expression for cooling capacity for radial wave geometry is

$$\bar{\dot{Q}}_2(\phi) =$$

$$\frac{\Omega\, k_0^2 A_{res}\, P_1(0)^2\, \beta T_0}{[2\rho_0 c\, k_0^2]} \left(\frac{J_0(\phi)J_1(\phi)}{\Omega} \frac{Im\,[F^*(\lambda_T)F^*(\lambda)]}{(1+N_{pr})\,|F(\lambda)|^2} + \frac{2J_1^{\,2}(\phi)}{\Omega^2} \frac{\tau}{\gamma-1} \frac{Im\{F^*(\lambda_T)+N_{pr}\,F(\lambda)\}}{(1-N_{pr}^2)\,|F(\lambda)|^2} \right) \qquad (22)$$

The plane wave result is also given by Eq. (22) with the replacements $J_0(\phi)\rightarrow cos(\phi)$ and $J_1(\phi)\rightarrow sin(\phi)$. Since use is made of the same working fluid and k_0 in the comparison of radial and plane geometries the quantity $[2\rho_0 c\, k_0^2]$ is common to both plane and radial refrigerators, so for simplicity, cooling capacities discussed below were computed using $[2\rho_0 c\, k_0^2]=1$. It has already been shown how to calculate all of the other parameters in Eq. (22).

Heat flow in Eq. (22) vanishes for a sufficiently large dimensionless temperature gradient defined as τ_{max}. Evaluating the nontrivial solution for $\bar{\dot{Q}}_2(\phi) \rightarrow 0$ yields

$$\tau_{max} = -\frac{1-N_{pr}}{2} \frac{P_1(\phi)}{\rho_0 c\, v_s(\phi)} (\gamma-1) \frac{Im\,[F^*(\lambda_T)F^*(\lambda)]}{Im\,\{F^*(\lambda_T)+N_{pr}\,F(\lambda)\}} \qquad (23)$$

The quantity τ_{max} is useful for comparison with values of τ and is analogous to the mean critical temperature gradient in Eq. (1). However, even for $\tau > \tau_{max}$, the thermoacoustic engine is not

necessarily acting as a prime mover.[1] There exists a range of τ values such that $\tau_{max} < \tau < \tau_{pm}$ where the engine is not a refrigerator or prime mover, where τ_{pm} is the minimal temperature gradient necessary for the prime mover to operate.[1]

Comparison of radial and plane wave refrigerators now turns to the mathematical and computational side. We define the best radial or plane wave refrigerator as the one which has the highest C_m. Following specification of the working fluid's γ, β, and N_{pr}, and the stack porosity Ω, values of λ_T, ϕ, and τ can be floated around using numerical techniques until they land on a specific unique set of critical values that produce a maximum of C_m. Cooling capacity and COP/COPc can be obtained using these critical values of λ_T, ϕ, and τ. Keep in mind that stack plate spacing can be determined from λ_T, stack location in the standing wave from ϕ, and both stack length d and refrigerator temperature difference from the combination of τ and the desired COPc.

Table 1 shows the results of C_1 optimization, where cooling capacity and COP/COPc are taken to be equally important, for helium as the working fluid. Computations were performed for stack porosities of Ω=0.7 and Ω=0.5. As Ω decreases, particle velocity in the stack must increase to ensure that volume velocity is continuous at the stack-resonator section interface. As noted in Table 1, radial inner has a higher value of λ_T than the others because larger values of λ_T correspond to less overall KE loss[19] and thus the stack position $r/a=\phi/(k_0 a)$ can be closer to the peak of thermoacoustic gain in Fig. 6b. Since heat flow is proportional to r for the radial stacks, the radial inner stack, which is at smaller r, must be pushed as far as possible away from the origin to achieve reasonable heat flow, though at a cost of increased viscous loss. The critical λ_T for the radial inner case is larger than the others to reduce these viscous losses. Decreasing stack porosity increases the optimal λ_T, again to circumvent KE loss.[19] Stack position is reported in Table 1 as r/a for radial wave and z/h for plane wave geometries. Note that the optimal stack positions are well away from the locations of maximum thermoacoustic gain in Figs. 6a and 6b due to the need for reducing KE dissipation. Low values of τ and τ/τ_{max} indicates that the stack favors cooling capacity over COP/COPc. Radial inner has the lowest τ and τ/τ_{max} for the same reason that this case had the largest λ_T. The stack with highest cooling capacity is radial inner. Note that decreasing stack porosity decreases cooling capacity and COP/COPc in all cases. Also note that the radial outer has highest COP/COPc. Finally, plane stacks have the largest C_1.

Having seen that small stack porosity compounds viscous losses, it is increased to Ω=0.9 to reduce these losses. Viscous losses can be reduced further by going to a molar mixture of 60%He 40%Ar for which the Prandtl number is taken to be N_{pr}=0.392. Also investigated are compromise refrigerators where cooling capacity is emphasized more than COP/COPc (m=0.5 in Eq. (20)), where they are on equal footing (m=1), and at a number of cases where COP/COPc is emphasized more than cooling capacity (m=1.5 to 4 at steps of 0.5). The findings are that plane

wave refrigerators have higher C_m when $1 \le m \le 5$, indicating that they perhaps are the best overall choice when COP/COPc must be emphasized more than cooling capacity; and that the radial wave inner stack has higher C_m when m=0.5 indicating that they perhaps are the best choice when cooling capacity is emphasized more than COP/COPc. Figure 7 clearly shows that increasing COP/COPc decreases cooling capacity for all of these acoustic refrigerators. Note that the radial outer case has the highest COP/COPc, though the plane case is very similar. The cooling capacity of the radial inner case is highest for small m, but the plane case is larger for large m. Figure 8 shows that λ_T increases as m increases, which implies that wider stack plate spacing reduces viscous losses and thus increases COP/COPc, but reduces cooling capacity since the optimal value for cooling capacity is λ_T=3.2.[3] Keeping in mind the ideal stack positions for obtaining high thermoacoustic gain and low KE losses due to gas viscosity as shown in Figs. 6a-6b, Fig. 9 shows that as COP/COPc is emphasized increasingly more than cooling capacity, the stack location migrates away from thermoacoustic gain and towards low KE loss.

For fixed COPc, Fig. 10 shows that the stack temperature gradient increases as COP/COPc is increasingly emphasized, or, equivalently, stack plate spacing $k_0 d=(\beta T_0)/(2|\tau|$ COPc) decreases. The influence of the thermoacoustic term (the third term of Eq. (20), which is opposite in sign to the first two terms) for work flow increases for larger $|\tau|$ which has the effect of increasing COP/COPc. Figure 11 bolsters this observation since $\tau/\tau_{max} \rightarrow 1$ when COP/COPc is emphasized much more than cooling capacity. Note that the radial inner case has the lowest τ/τ_{max} which is consistent with this case producing high cooling capacities and low COP/COPc. Radial outer and plane cases have very similar τ/τ_{max} ratios.

B. Comparison of radial and plane wave prime movers.

Prime movers begin to make sound when a sufficiently large temperature gradient is established across the stack.[1,3,4,10-13] Acoustic power generated by the stack must be large enough to overcome thermal and viscous losses occurring in the stack, heat exchanger, and resonator sections, and possibly to provide power for an acoustic load. The first two terms of Eq. (18) describe dissipation of potential and kinetic energy in the stack. Equation (18) does not take into account acoustic power dissipation in heat exchangers and resonator sections, or acoustic power that might flow out of the resonator when the prime mover is being used as a sound source for another device. All such dissipation is swept into a single inherently positive quantity $\bar{\dot{W}}_{ext}$. Hence the thermoacoustic sound source begins to operate when the temperature gradient is sufficiently large that the inequality

$$\bar{\dot{W}}_2(\phi) + \bar{\dot{W}}_{ext} \le 0 \qquad (24)$$

is satisfied.[4] Define a dimensionless external work $\bar{\dot{w}}_{ext}$ flow,

$$\bar{\dot{w}}_{ext} \equiv \frac{2\rho_0 c^2}{V_G P_1(0)^2 \omega} \bar{\dot{W}}_{ext} \quad . \tag{25}$$

For example, in a helium filled plane wave resonator containing a fairly optimal prime mover stack, a value $\bar{\dot{w}}_{ext} = 0.52$ was determined.[4]

The magnitude of each term in Eq. (18) is determined by the phase angle ϕ, the stack plate spacing surrogate λ_T, and thermal and transport properties of the working fluid. The dimensionless stack temperature gradient τ is given in Eq. (19). For the proper choice of stack placement there exists a minimal value $\tau_{min}(\phi_{min},\lambda_T)$ necessary for onset as a solution of Eq. (24). In previous work, it was shown that the minimal value of the nondimensional temperature gradient for onset of oscillation for the plane wave geometry was[4]

$$\tau_{min} = \pm \Omega \frac{1 - N_{pr}}{Im\ \{F^*(\lambda_T)/F^*(\lambda)\}} \sqrt{[(\gamma - 1)\ Im\ F^*(\lambda_T) + \bar{\dot{w}}_{ext}][Im\ F^*(\lambda)/|\Omega F(\lambda)|^2 + \bar{\dot{w}}_{ext}]}\ , \tag{26}$$

where the positive solution applies when the sign of the product of pressure and particle velocity in the standing wave is negative. Stack placement in the standing wave is determined by the phase angle corresponding to the minimum onset temperature gradient in Eq. (26):

$$tan\ (\phi_{min}) = \sqrt{\frac{(\gamma - 1)\ Im\ F^*(\lambda_T) + \bar{\dot{w}}_{ext}}{Im\ F^*(\lambda)/|\Omega F(\lambda)|^2 + \bar{\dot{w}}_{ext}}}\ , \tag{27}$$

where ϕ_{min} [π - ϕ_{min}] is the phase angle that corresponds to the negative [positive] solution for τ_{min} in Eq. (26) (the plane inner [plane outer] in Fig. 2b).

A similar analysis can be performed for determining τ_{min} in the radial wave geometry; however, a closed form solution for the general case has not been found. Solving Eq. (24) for τ yields

$$\tau = -\frac{\Omega(1 - N_{pr})}{Im\ \{F^*(\lambda_T)/F^*(\lambda)\}}\ X$$

$$\left(\frac{\bar{\dot{W}}_{ext}}{2J_0(\phi)J_1(\phi)} + (\gamma - 1)\, Im\, F^*(\lambda_T) \frac{J_0(\phi)}{2J_1(\phi)} + \frac{Im\, F^*(\lambda)}{|\Omega F(\lambda)|^2} \frac{J_1(\phi)}{2J_0(\phi)} \right) , \tag{28}$$

where the reader might note the close correspondence with Eq. (6) of Ref. 4. The derivative of Eq. (28) with respect to ϕ is

$$G(\phi) = \bar{\dot{w}}_{ext} \left(J_0{}^2(\phi) - J_1{}^2(\phi) \right) + \left(J_0{}^2(\phi) - \frac{J_0(\phi)J_1(\phi)}{\phi} + J_1{}^2(\phi) \right) X$$

$$\left((\gamma - 1)\, Im\, F^*(\lambda_T)\, J_0{}^2(\phi) - \frac{Im\, F^*(\lambda)}{|\Omega F(\lambda)|^2} J_1{}^2(\phi) \right) , \tag{29}$$

from which ϕ_{min} is determined by solving $G(\phi_{min}) = 0$ with numerical techniques. Then

$$\tau_{min} = \tau(\phi_{min}) \tag{30}$$

is the desired minimal value of the dimensionless temperature gradient that is needed for a radial wave prime mover to operate. The radial inner and radial outer cases in Fig. 2 can be evaluated by choosing appropriate initial values for ϕ.

The optimal temperature gradients τ_{min} for plane and radial wave geometries in Eqs. (26) and (30) are functions of λ_T. Figure 4b of Ref. 4 shows that $\tau_{min}(\lambda_T)$ has a unique minimum for the proper choice λ_T. Numerical techniques can be used to obtain the minimum value of τ_{min} as a function of λ_T for the general case of arbitrary $\bar{\dot{W}}_{ext}$. Thus there is now a procedure for obtaining the lowest possible operating temperature gradient necessary to deliver a given amount of acoustic power by adjusting engine properties of stack location in the standing wave and stack plate spacing. One criterion for finding the "best" geometry is to find the stack in radial or plane geometry which has the smallest τ_{min} for given $\bar{\dot{W}}_{ext}$.

Several assumptions are necessary to compare prime movers in radial and plane wave geometry, in addition to those given in Sec. III. Stack work flow in Eq. (18) is linearly proportional to stack length so for the comparison equal stack lengths are assumed. The actual acoustic load $\bar{\dot{W}}_{ext}$ that must be delivered by either plane or radial wave stacks is assumed to be the same. Using these two assumptions along with the relations $k_0h = \pi$ and $k_0a = 3.832$ that describe the resonator geometries, and the normalization for $P_1(0)$ for radial and plane wave geometries as discussed in Sec. III, the relation between scaled external work for radial and plane geometries is

$$\bar{\dot{w}}_{ext,r} = \bar{\dot{w}}_{ext,p} \frac{0.7581}{k_0 r} , \tag{31}$$

where $k_0 r = \phi$ is the phase angle of the radial stack, and the subscripts p and r refer to plane and radial wave geometries. Equation (31) is used to obtain the scaled external work for the radial stack that corresponds to a given plane wave geometry external work. A measure of engine performance is efficiency defined as

$$\eta_r , \eta_p \equiv \frac{\bar{\dot{W}}_{ext}}{\bar{\dot{Q}}_2} . \tag{32}$$

The ratio η_r/η_p of radial to plane wave efficiencies is presented below.

Figure 12 shows values of λ_T that minimize τ_{min} for the radial outer, radial inner, plane outer, and plane inner stacks in Fig. 2. The inset graph shows that λ_T is the same for all stacks when $\bar{\dot{w}}_{ext,p} \rightarrow 0$. Viscous losses in the stack, given by the second term of Eq. (18), are the dominant loss mechanism in this limit, and can be reduced by choosing the plate spacing such that $\lambda_T >> 3.2$. However, thermoacoustic gain is largest for $\lambda_T \approx 3.2$. The optimal choice for λ_T is a trade-off between viscous loss and thermoacoustic gain. As $\bar{\dot{w}}_{ext,p}$ increases, viscous losses in the stack no longer dominate the acoustic load that must be delivered by thermoacoustic gain, so $\lambda_T \approx 3.2$ determines the optimal plate spacing to use.

The optimal stack location, determined from Eq. (27) for plane and Eq. (29) for radial wave geometry, is shown in Fig. 13 as a function of $\bar{\dot{w}}_{ext,p}$. By symmetry, the plane wave stacks are the same distance from resonator walls located at z/h=0 and at z/h=1. For $\bar{\dot{w}}_{ext,p} \rightarrow 0$, viscous losses can be reduced by moving the stack closer to velocity nodes, though some thermoacoustic gain is sacrificed (see Figs. 6a and 6b). As $\bar{\dot{w}}_{ext,p}$ increases, viscous losses in the stack no longer dominate the acoustic load that must be delivered by thermoacoustic gain, so the optimal stack positions approach the positions for maximal thermoacoustic gain shown in Figs. 6a and 6b.

The dimensionless temperature gradients for onset are shown in Fig. (14). Values for plane and radial geometries were obtained using Eqs. (26) and (30). The inset graph shows that $|\tau_{min}|$ is the same for all stacks in the limit $\bar{\dot{w}}_{ext,p} \rightarrow 0$, which can easily be shown from use of Eqs. (26) and (30). The sign of τ_{min} is determined from the requirement that the hot end of the stacks in Figs. 2a and 2b must face pressure antinodes so that the third term of Eq. (18) provides gain (if the direction of the temperature gradients were reversed, the stack would only provide

loss). Note that the radial inner stack has the lowest $|\tau_{min}|$, and in this sense, is a better choice than the other stacks. Based on the critical temperature gradients show in Fig. 3, one would have guessed that radial outer would have the lowest $|\tau_{min}|$, and radial inner the highest, so at first glance, the results in Fig. (14) are counterintuitive. However, the critical temperature gradients in Fig. 3 do not account for viscous losses that depend on the square of particle velocity. Careful examination of Figs. 6a and 6b shows that radial inner has the highest ratio of thermoacoustic gain to kinetic energy (viscous) loss, followed by plane and radial outer, and hence this ratio largely determines that radial inner has the lowest $|\tau_{min}|$. Also note that this ratio is inversely proportional to the critical mean-temperature gradients of Fig. 3.

Efficiency ratios of radial inner and radial outer to plane are shown in Fig. 15 as a function of the scaled external work that must be delivered by the plane stack. Note that the radial outer stack generally is slightly more efficient than the plane wave stacks, and the radial inner is only more efficient than the plane wave stacks when $\bar{\dot{w}}_{ext,p} \rightarrow 0$. For efficiency considerations alone the radial outer appears to be the optimal choice.

IV. CONCLUSION

A general linear framework was developed for analyzing radial wave thermoacoustic engines. Pressure and specific acoustic impedance translation equations were developed for the various thermoacoustic elements, and the stack enthalpy flow can be expressed in terms of these quantities. Theory for the use of thermoacoustic engines to enhance the signal to noise ratio of photoacoustic spectrometers was developed. In this example it was noted that the dependence of resonance frequency on stack plate spacing can be very different, depending on whether a temperature gradient is applied across the stack. The thermoacoustic enhanced photoacoustic spectrometer was likened to an analog amplifier with amplification Q, bandwidth f_0/Q, and discrimination against Gaussian acoustic noise (signal to noise ratio) $Q^{1/2}$, where f_0 is the resonance frequency and Q is the quality factor.

The short stack approximation was given for radial and plane wave geometries, and was used to compare the performance of refrigerators and prime movers (or sound sources) constructed using these stacks. Refrigerator performance was evaluated using the weighted product of cooling capacity and coefficient of performance as a measure of capability. Prime movers were compared using a given acoustic power as a load and the criterion that a minimal onset temperature gradient and high efficiency are indicators of good thermoacoustic sound sources. Independent parameters for both refrigerators and prime movers were stack plate spacing and stack location in the standing wave. Refrigerators had stack length as an additional independent parameter. Results of the comparison are that engines in the plane wave geometry are better overall refrigerators when maximizing both cooling capacity and coefficient of

performance, though radial stacks placed near the resonator center can have higher cooling capacities and radial stacks near the resonator wall have slightly higher coefficients of performance. The radial wave geometry yields prime movers with lower temperature gradients and higher efficiency for a given acoustic power load. For both refrigerators and sound sources it was noted that to improve thermoacoustic engine performance, the viscous losses associated with the square of particle velocity need to be lowered without sacrificing too much desirable thermoacoustic gain associated with the product of particle velocity and acoustic pressure. Finally, the radial analysis and intuition developed here is qualitatively applicable to nominally plane wave resonators where the resonator radius increases along the axis.

Acknowledgments

This work was supported by the Office of Naval Research in association with the Environmentally Safe Ships Program (ESSP). W. P. Arnott and H. Moosmüller are also supported for the photoacoustic application by the Environmental Protection Agency, Office of Exploratory Research. The authors thank Henry E. Bass for his suggestions and contributions to this research. Jeffery R. Olson made helpful suggestions for the refrigerator comparisons and critically read the manuscript.

REFERENCES

1. G. W. Swift, "Thermoacoustic engines," J. Acoust. Soc. Am. **84**, 1145-1180 (1988).
2. N. Rott, "Thermoacoustics," Adv. Appl. Mech. **20**, 135-175, (1980).
3. W. P. Arnott, H. E. Bass, and R. Raspet, "General formulation of thermoacoustics for stacks having arbitrarily shaped pore cross sections," J. Acoust. Soc. Am. **90**, 3228-3237 (1991).
4. W. P. Arnott, J. R. Belcher, R. Raspet, and H. E. Bass, "Stability analysis of a helium-filled thermoacoustic engine," J. Acoust. Soc. Am. **96**, 370-375, (1994).
5. W. P. Arnott, H. Moosmüller, R. Purcell, J. Lightfoot, R. Raspet, and H. E. Bass, "Thermoacoustic enhancement and control of the quality factor in a resonant photoacoustic cell for measurement of light absorption by aerosols and gases," J. Acoust. Soc. Am. Suppl., **95**, S2811.
6. A. D. Pierce, *Acoustics: An Introduction to Its Physical Principles and Applications* (American Institute of Physics, New York, 1989).
7. W. C. Chew, *Waves and Fields in Inhomogeneous Media,* (Van Nostrand Reinhold, New York, 1990) 161-182.
8. D. K. Holger, "The attenuation of sound propagating through a radial diffuser with absorptive walls," J. Sound Vib. **79**, 1-9 (1981).
9. Comparison of the notation used here and in Ref. 3 with that used in Ref. 1 is discussed in the paragraph following Eq. (48) in Ref. 3.
10. A. A. Atchley, H. E. Bass, T. J. Hofler, and H. T. Lin, "Study of a thermoacoustic prime mover below onset of self-oscillation," J. Acoust. Soc. Am. **91**, 734-743 (1992).
11. A. A. Atchley and F. M. Kuo, "Stability curves for a thermoacoustic prime mover," J. Acoust. Soc. Am. **95**, 1401-1404 (1994).
12. A. A. Atchley, "Standing wave analysis of a thermoacoustic prime mover below onset of self-oscillation," J. Acoust. Soc. Am. **92**, 2907-2914 (1992).
13. A. A. Atchley, "Analysis of the initial buildup of oscillations in a thermoacoustic prime mover," J. Acoust. Soc. Am. **95**, 1661-1664 (1994).
14. P. M. Morse and K. U. Ingard, *Theoretical Acoustics,* (Princeton University Press, Princeton, New Jersey, 1986) 519-522.
15. K. M. Adams, "Real-time *in situ* measurements of atmospheric optical absorption in the visible via photoacosutic spectroscopy. 1: Evaluation of photoacostic cells," Appl. Opt., **27**, 4052-4056 (1988).
16. R. Gerlach and N. M. Amer, "Brewster window and windowless resonant spectrophones for intracavity operation," Appl. Phys. **23**, 319-326.

17. W. P Arnott, R. Raspet, and H. E. Bass, "Thermoacoustic engines," Proc. IEEE 1991 Ultrasonics Symp. **2**, 995-1003 (1991). The last term of Eq. (6) should be *Im* $\{F^*(\lambda_T)/F^*(\lambda)\}$.

18. J. R. Olson and G. W. Swift, "Similitude in thermoacoustics," J. Acoust. Soc. Am. **95**, 1405-1412.

19. Kinetic energy loss in Eq. (20) is proportional to *Im* $F^*(\lambda)$. As shown in Fig. 5 of Ref. 3, $|Im\ F(\lambda)| \rightarrow 0$ as $\lambda \rightarrow \infty$. Hence KE dissipation diminishes as λ increases beyond $\lambda \approx 3.2$. However, the desired thermoacoustic gain is roughly proportional to *Im* $F^*(\lambda_T)$, and the largest value of *Im* $F^*(\lambda_T)$ occurs for $\lambda_T \approx 3.2$. Keep in mind that $\lambda_T = N_{pr}^{1/2}\lambda$, so usually $\lambda_T < \lambda$. Hence the choice of optimal λ_T is balanced by a trade off between the optimal value λ_T=3.2 for thermoacoustic gain and the desire for low KE dissipation by gas viscosity which occurs for $\lambda >> 3.2$.

TABLE

Table 1. Optimized refrigerator parameters for Helium as working fluid.

Quantity	Radial Inner Ω=70% (Ω=50%)	Plane Ω=70% (Ω=50%)	Radial Outer Ω=70% (Ω=50%)
λ_T	4.062 (4.150)	3.858 (3.900)	3.828 (3.871)
$\frac{r}{a}$ or $\frac{z}{h}$	0.220 (0.196)	0.096 (0.075)	0.928 (0.943)
τ	-0.168 (-0.134)	-0.266 (-0.243)	0.281 (0.256)
$\frac{\tau}{\tau_{max}}$	0.382 (0.371)	0.408 (0.403)	0.411 (0.406)
$\bar{\dot{Q}}_2(\phi)$	**18.50 (15.49)**	14.60 (11.71)	10.68 (8.69)
$\frac{COP}{COPc}$	0.162 (0.126)	0.244 (0.228)	**0.254 (0.237)**
C_1	2.988 (1.955)	**3.560 (2.665)**	2.715 (2.062)

FIGURE CAPTIONS

1. Possible arrangements for a radial wave thermoacoustic engines. Cold heat exchangers face the pressure nodes. The three regions used in analysis are shown. The z axis (not shown) is perpendicular to the plane of the paper. Distance d is shown as the cold heat exchanger length and is generally used to represent the length of any thermoacoustic element.

2. Coordinate system and stack locations (e.g. Radial Inner, etc.) for a) radial and b) plane wave resonators. Resonator height is h and radius is a. Particle velocity is in the r direction in a) and is in the z direction in b).

3. Dimensionless critical temperature gradient for plane (dashed line) and radial wave engines (full line).

4. Conceptual design of a thermoacoustic enhanced photoacoustic spectrometer.

5. a) Resonance frequency and b) quality factor of a radial wave prime mover below the onset of oscillation, as a function of stack and heat exchanger plate spacing, R. The light, medium, and heavy weight curves labeled in a) as 0.8d, d = 3.28 mm, and 1.2d all are for $T_{0\infty}$ = 26.6 K/mm. The medium weight curves in a) and b) labeled d, $T_{0\infty} = 0$, are for no temperature gradient on the stack of length d, and the entire resonator at the ambient temperature. The dashed lines are for a resonator with no stack or heat exchangers.

6. Stack thermoacoustic gain, and losses of kinetic and potential energy, as a function of stack position in a) a plane wave resonator, and b) a radial wave resonator. Numbers on the graphs indicate positions of relative extrema of thermoacoustic gain. Though not shown as such, KE losses due to gas viscosity are usually more severe than PE losses due to gas thermal conductivity.

7. Cooling capacities and Coefficient of Performance ratios as a function of the emphasis, m, on Coefficient of Performance. Calculation points are shown by the symbols and the lines connect these points for viewing ease. Solid symbols are cooling capacity, squares refer to radial inner stacks, triangles to radial outer, and circles to plane stacks. COP/COPc nearly overlap for plane and radial outer.

8. Thermal disturbance numbers λ_T as a function of the emphasis, m, on Coefficient of Performance. The inset graph shows that λ_T is the same for all when the stack has no external work load. Symbols are the same as in Figure 8.

9. Stack locations as a function of the emphasis, m, on Coefficient of Performance. Symbols are the same as in Figure 8.

10. Nondimensional temperature gradients τ as a function of the emphasis, m, on Coefficient of Performance. Symbols are the same as in Figure 8.

11. Ratios of the nondimensional temperature gradient τ to the maximum possible value for refrigeration, τ_{max}, as a function of the emphasis, m, on Coefficient of Performance. Symbols are the same as in Figure 8. The radial outer and plane results nearly overlap.

12. Thermal disturbance number λ_T as a function of the external work load that must be delivered by the stack in radial (doubly thick lines) and plane wave resonators. The inset graph shows that λ_T is the same for all cases when the stack has no external work load.

13. Optimal stack location for varying external work load. Radial wave stack locations are given by doubly thick lines.

14. The optimal nondimensional temperature gradient τ_{min} as a function of external work that must be delivered by the stack. Doubly thick lines are for the radial wave cases. The inset graph shows in more detail that τ_{min} is the same for either the plane or radial wave resonators when the stack has no external work load.

15. Ratio of radial wave efficiencies to plane wave efficiency as a function of the normalized external work flow for the plane wave resonator.

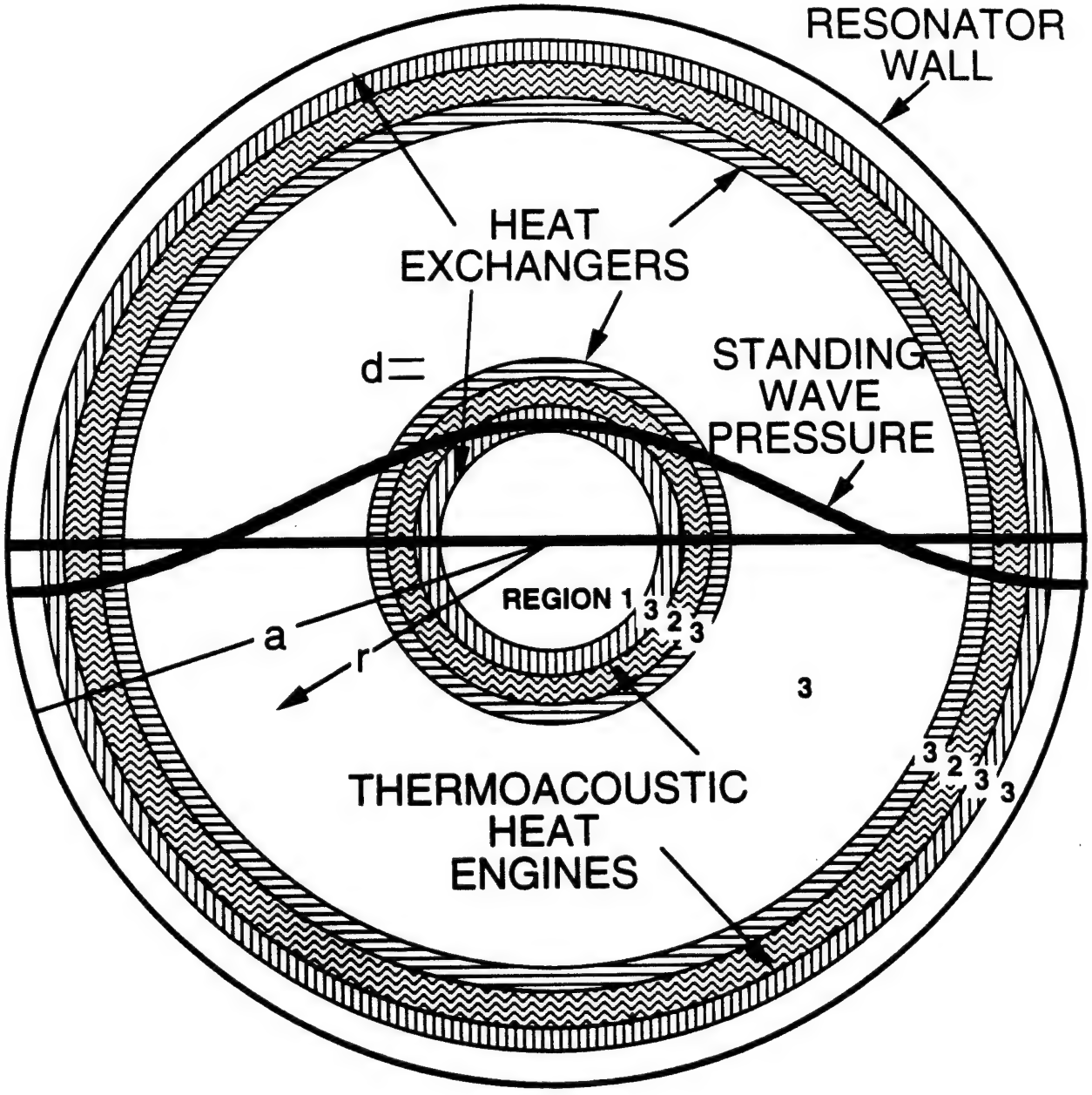
RESONATOR
WALL
HEAT
EXCHANGERS
d=
STANDING
WAVE
PRESSURE
REGION 1
3
2
3
a
r
3
3
2
3
3
THERMOACOUSTIC
HEAT
ENGINES

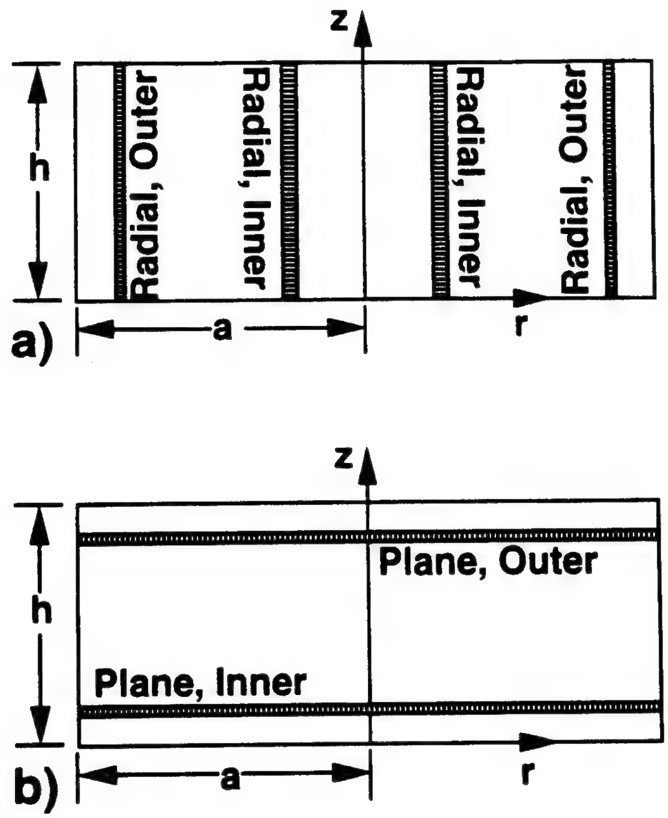
z
h
Radial, Outer
Radial, Inner
Radial, Inner
Radial, Outer
a)
a
r
z
h
Plane, Outer
Plane, Inner
b)
a
r

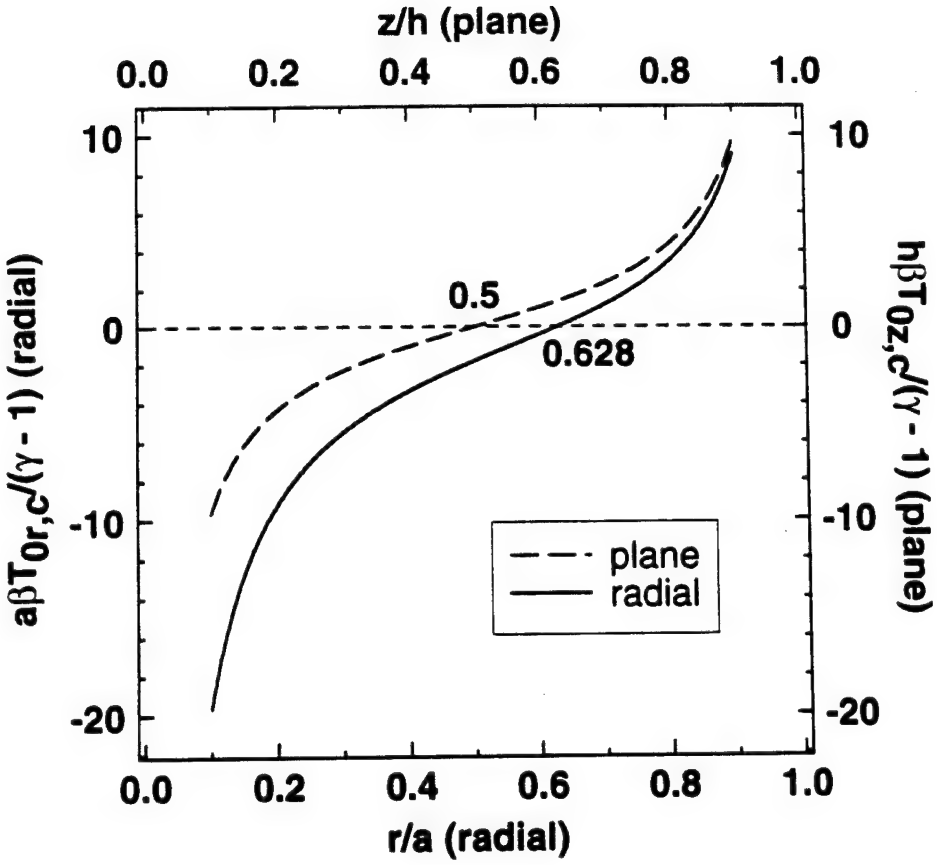
z/h (plane)
0.0
0.2
0.4
0.6
0.8
1.0
10
0
-10
-20
0.5
0.628
plane
radial
aβT0r,c/(γ - 1) (radial)
hβT0z,c/(γ - 1) (plane)
r/a (radial)

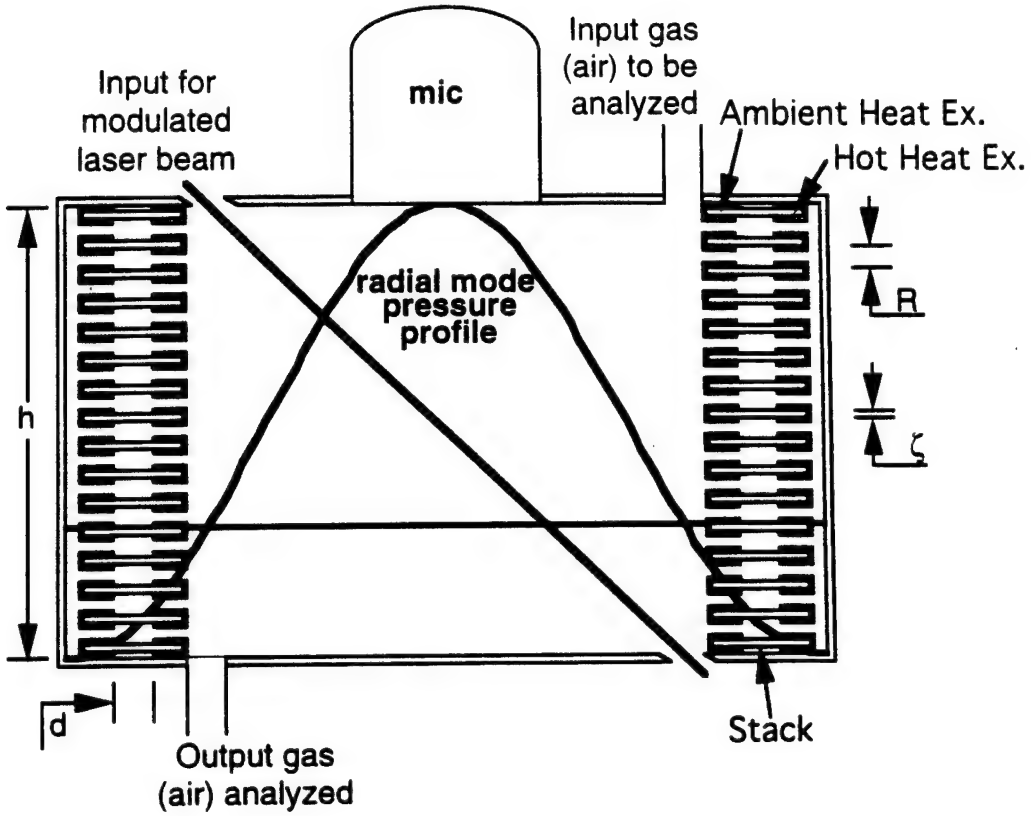
Input for
modulated
laser beam
mic
Input gas
(air) to be
analyzed
Ambient Heat Ex.
Hot Heat Ex.
radial mode
pressure
profile
h
R
ζ
d
Output gas
(air) analyzed
Stack

Fig 4

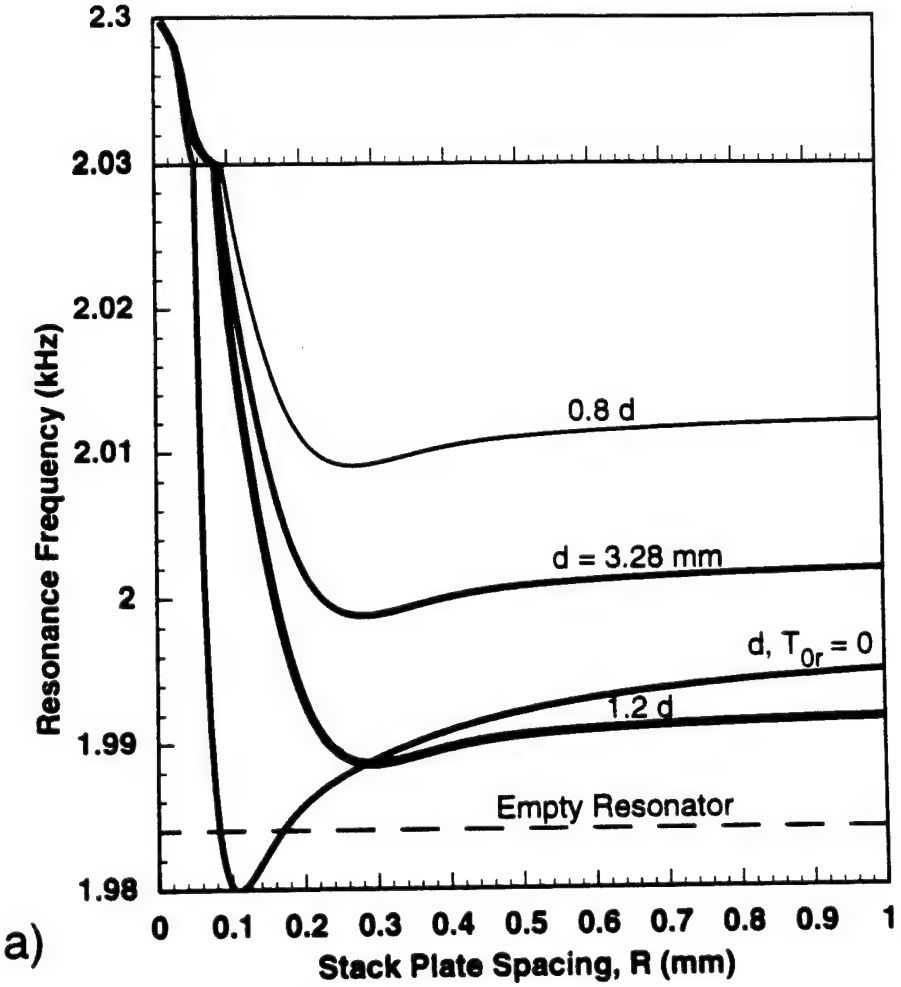
2.3
2.03
2.02
2.01
2
1.99
1.98
Resonance Frequency (kHz)
0.8 d
d = 3.28 mm
d, T_{0r} = 0
1.2 d
Empty Resonator
0
0.1
0.2
0.3
0.4
0.5
0.6
0.7
0.8
0.9
1
Stack Plate Spacing, R (mm)

a)

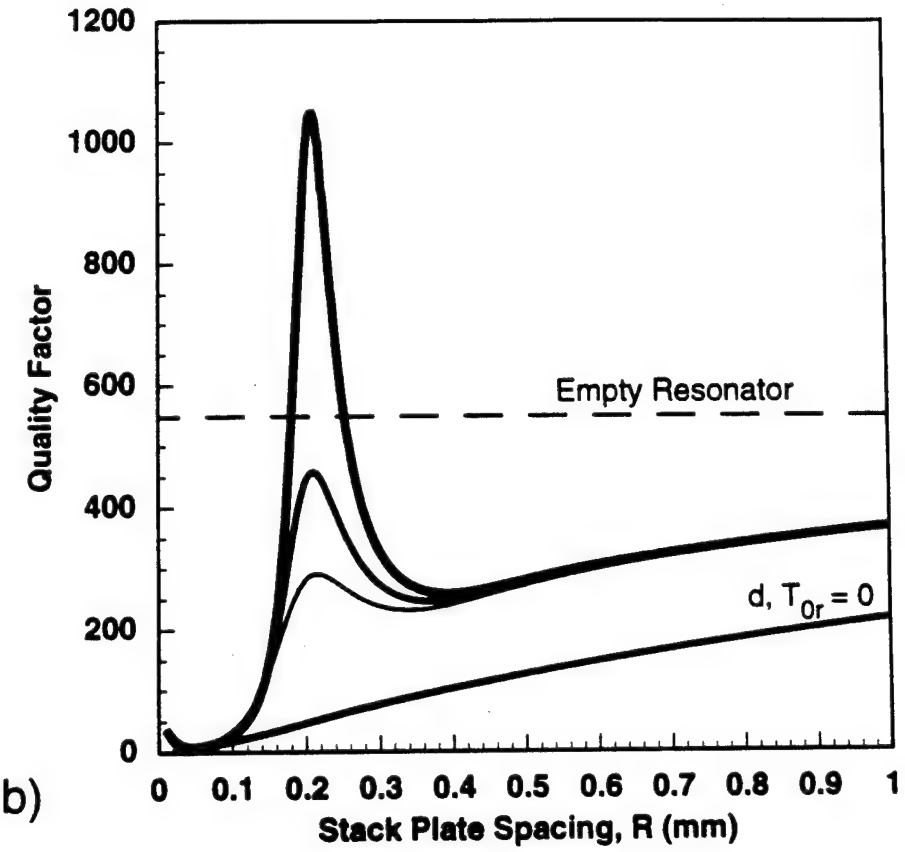
1200
1000
800
600
400
200
0
Quality Factor
Empty Resonator
d, T_{0r} = 0
0
0.1
0.2
0.3
0.4
0.5
0.6
0.7
0.8
0.9
1
Stack Plate Spacing, R (mm)

b)

Fig 5b

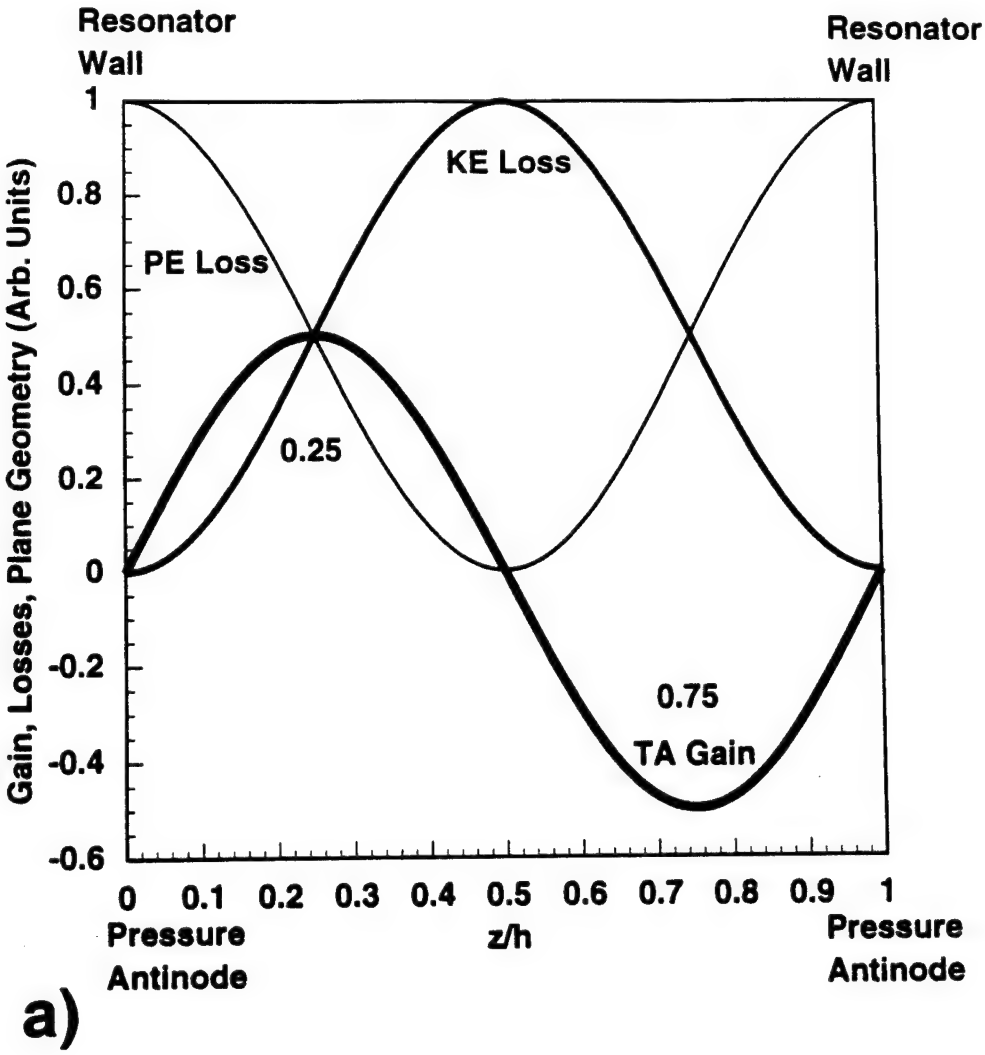
Resonator Wall
Resonator Wall
KE Loss
PE Loss
0.25
0.75
TA Gain
Gain, Losses, Plane Geometry (Arb. Units)
1
0.8
0.6
0.4
0.2
0
-0.2
-0.4
-0.6
0 0.1 0.2 0.3 0.4 0.5 0.6 0.7 0.8 0.9 1
z/h
Pressure Antinode
Pressure Antinode

a)

Fig 6A

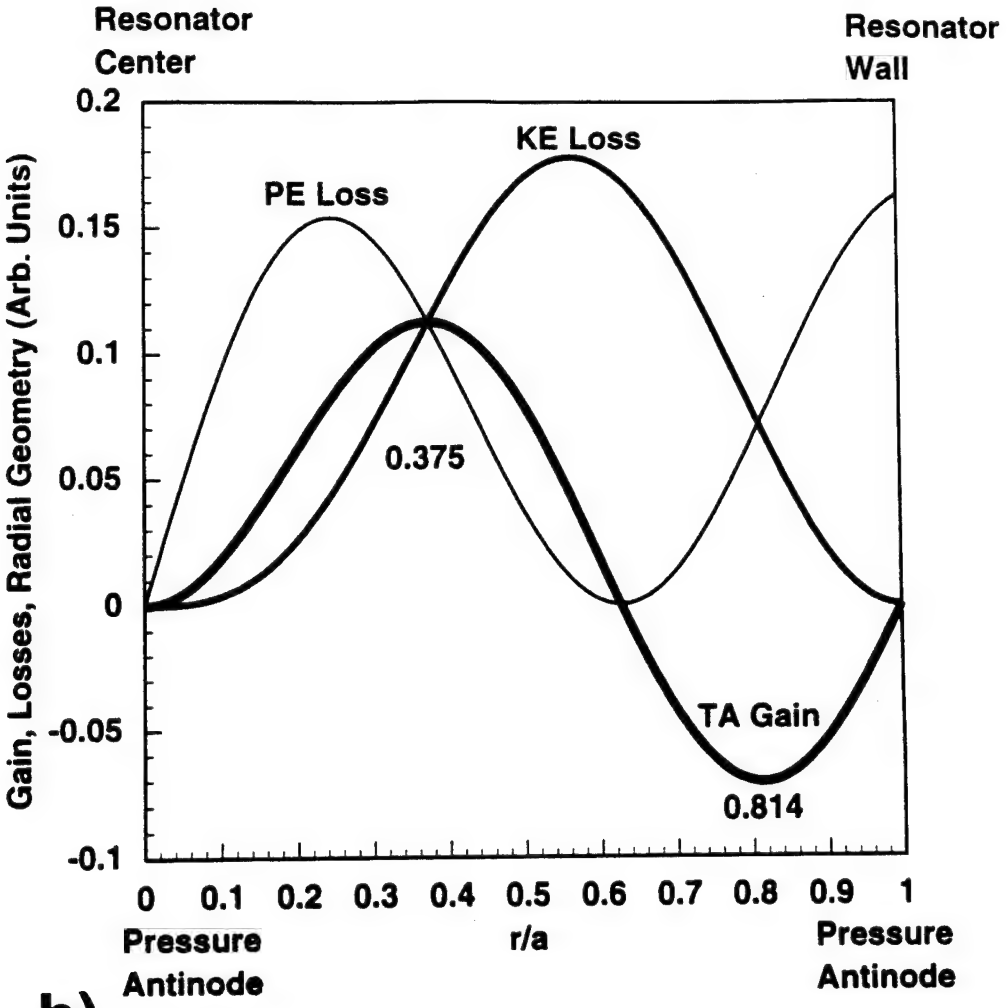
Resonator
Center
Resonator
Wall
0.2
0.15
0.1
0.05
0
-0.05
-0.1
Gain, Losses, Radial Geometry (Arb. Units)
KE Loss
PE Loss
0.375
TA Gain
0.814
0
0.1
0.2
0.3
0.4
0.5
0.6
0.7
0.8
0.9
1
r/a
Pressure
Antinode
Pressure
Antinode

b)

Fig 6B

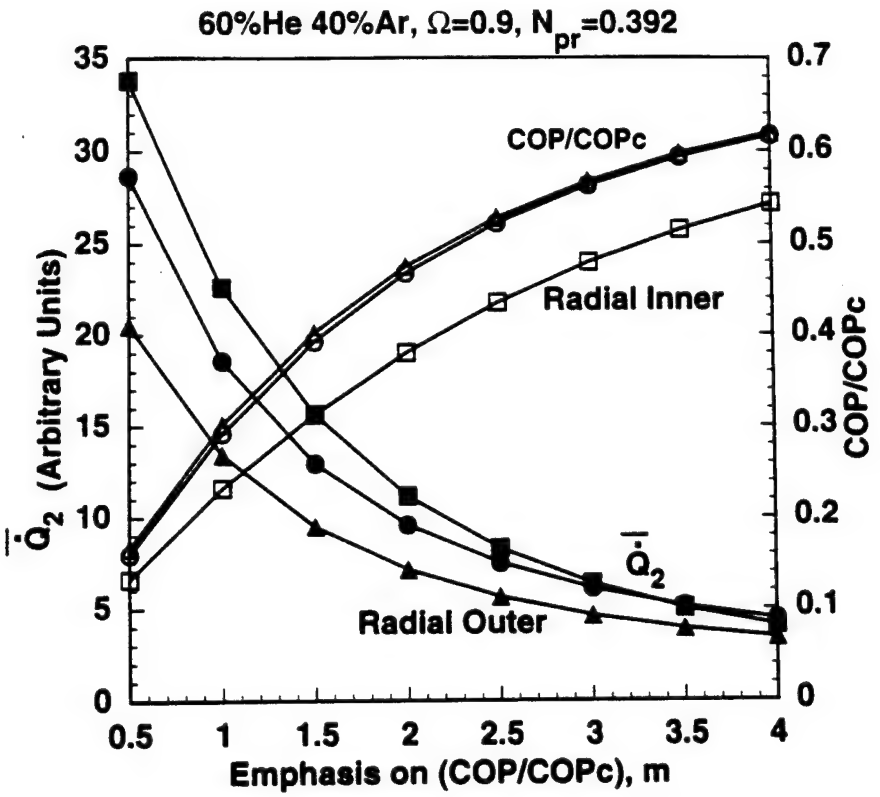
60%He 40%Ar, Ω=0.9, N_pr=0.392
35
30
25
20
15
10
5
0
0.7
0.6
0.5
0.4
0.3
0.2
0.1
0
COP/COPc
Radial Inner
Radial Outer
$\overline{\dot{Q}}_2$
$\overline{\dot{Q}}_2$ (Arbitrary Units)
COP/COPc
0.5
1
1.5
2
2.5
3
3.5
4
Emphasis on (COP/COPc), m

Fig 7

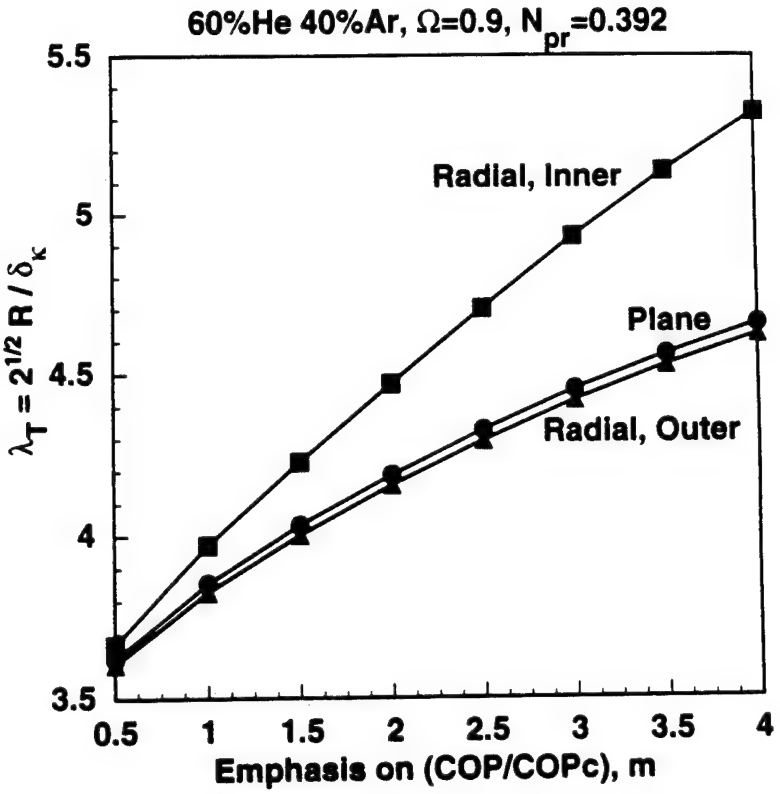
60%He 40%Ar, Ω=0.9, N_pr=0.392
5.5
5
4.5
4
3.5
λ_T = 2^1/2 R / δ_κ
Radial, Inner
Plane
Radial, Outer
0.5
1
1.5
2
2.5
3
3.5
4
Emphasis on (COP/COPc), m

Fig. 5

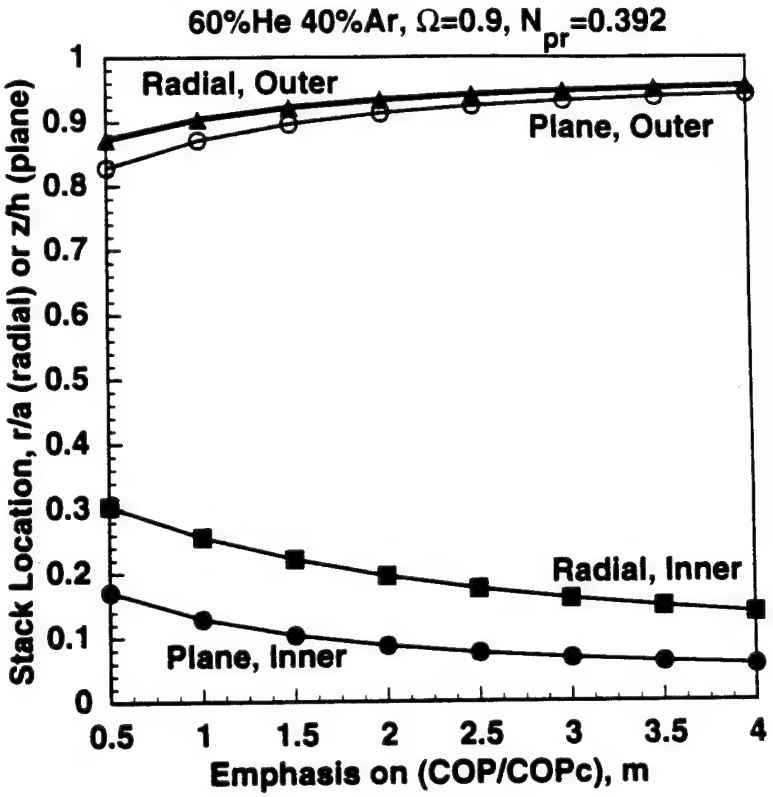
60%He 40%Ar, Ω=0.9, N_pr=0.392
Radial, Outer
Plane, Outer
Radial, Inner
Plane, Inner
Stack Location, r/a (radial) or z/h (plane)
Emphasis on (COP/COPc), m
0
0.1
0.2
0.3
0.4
0.5
0.6
0.7
0.8
0.9
1
0.5
1
1.5
2
2.5
3
3.5
4

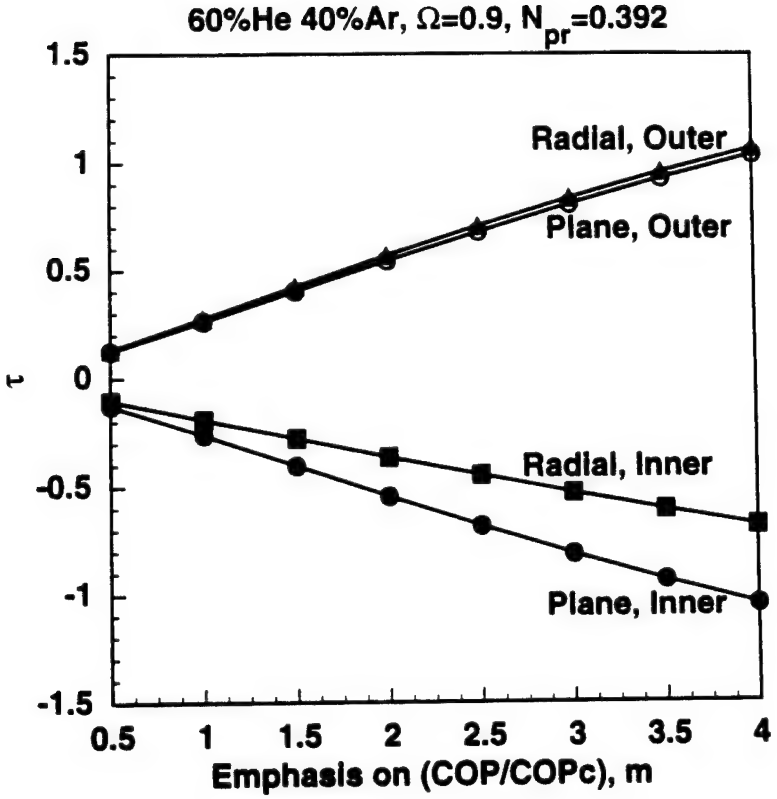
60%He 40%Ar, Ω=0.9, N_pr=0.392
1.5
1
0.5
0
-0.5
-1
-1.5
τ
Radial, Outer
Plane, Outer
Radial, Inner
Plane, Inner
0.5
1
1.5
2
2.5
3
3.5
4
Emphasis on (COP/COPc), m

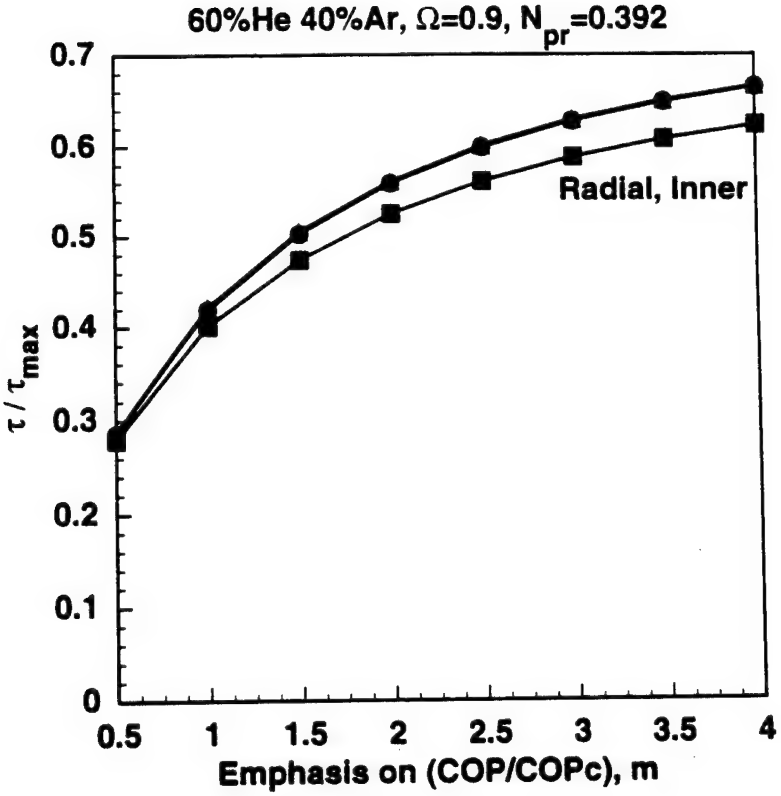
60%He 40%Ar, Ω=0.9, N_pr=0.392
0.7
0.6
0.5
0.4
0.3
0.2
0.1
0
τ / τ_max
Radial, Inner
0.5
1
1.5
2
2.5
3
3.5
4
Emphasis on (COP/COPc), m

Fig 11

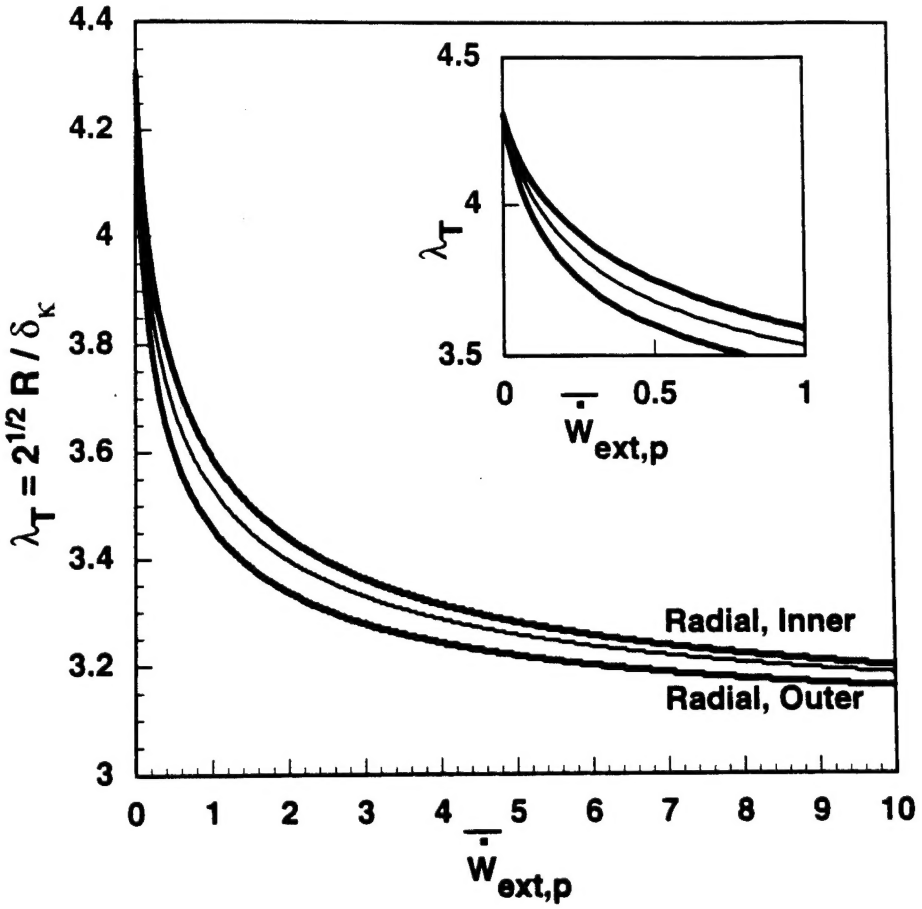
4.4
4.2
4
3.8
3.6
3.4
3.2
3
$\lambda_T = 2^{1/2} R / \delta_\kappa$
0
1
2
3
4
5
6
7
8
9
10
$\dot{W}_{ext,p}$
Radial, Inner
Radial, Outer
4.5
4
3.5
λ_T
0
0.5
1
$\dot{W}_{ext,p}$

Fig 12

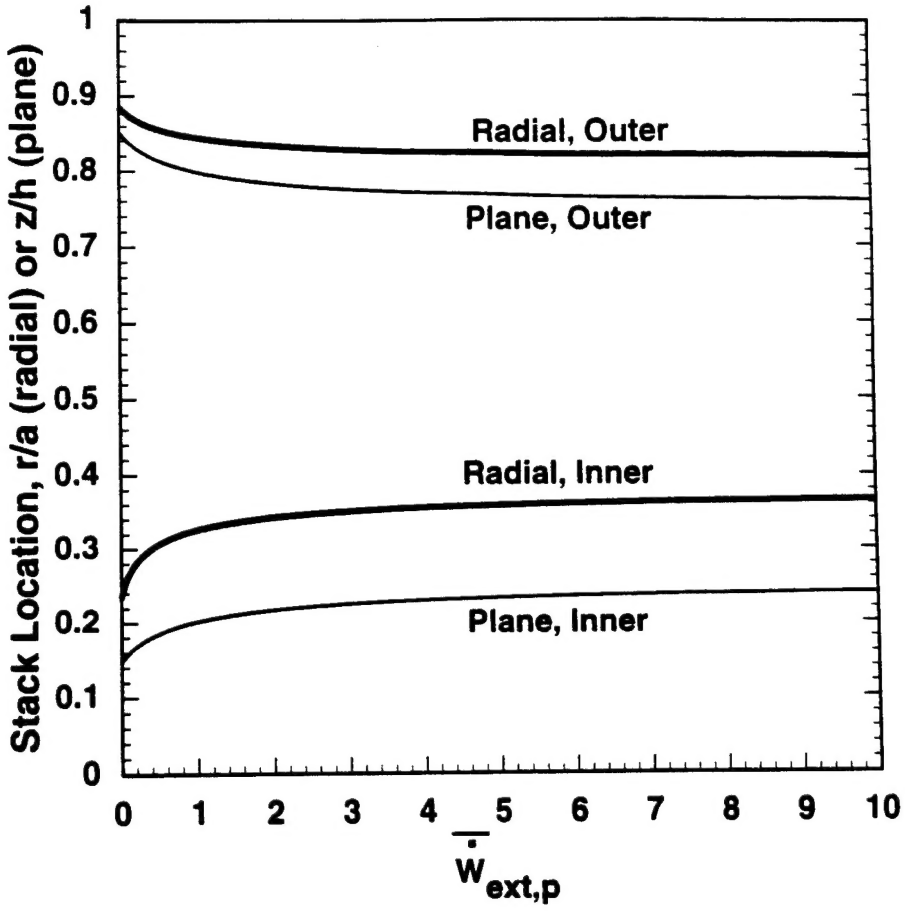
Stack Location, r/a (radial) or z/h (plane)
1
0.9
0.8
0.7
0.6
0.5
0.4
0.3
0.2
0.1
0
Radial, Outer
Plane, Outer
Radial, Inner
Plane, Inner
0
1
2
3
4
5
6
7
8
9
10
$\overline{\dot{W}}_{ext,p}$

Fig 13

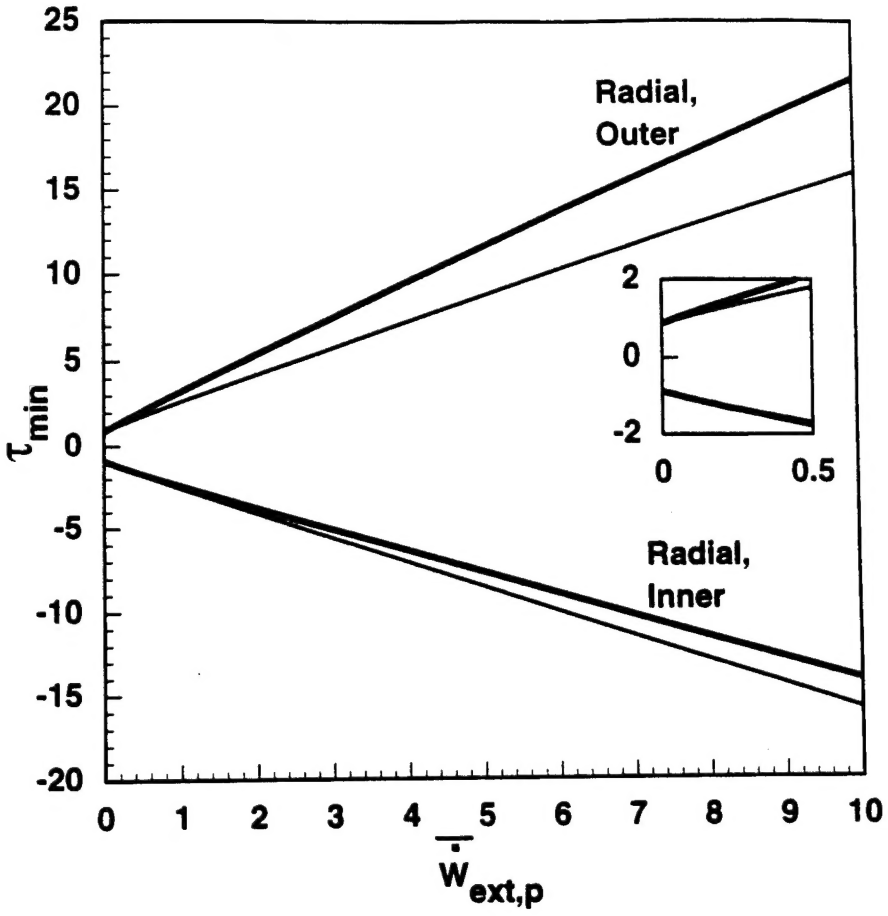
25
20
15
10
5
0
-5
-10
-15
-20
τ_{min}
Radial,
Outer
Radial,
Inner
2
0
-2
0
0.5
0
1
2
3
4
5
6
7
8
9
10
$\dot{W}_{ext,p}$

Fig 14

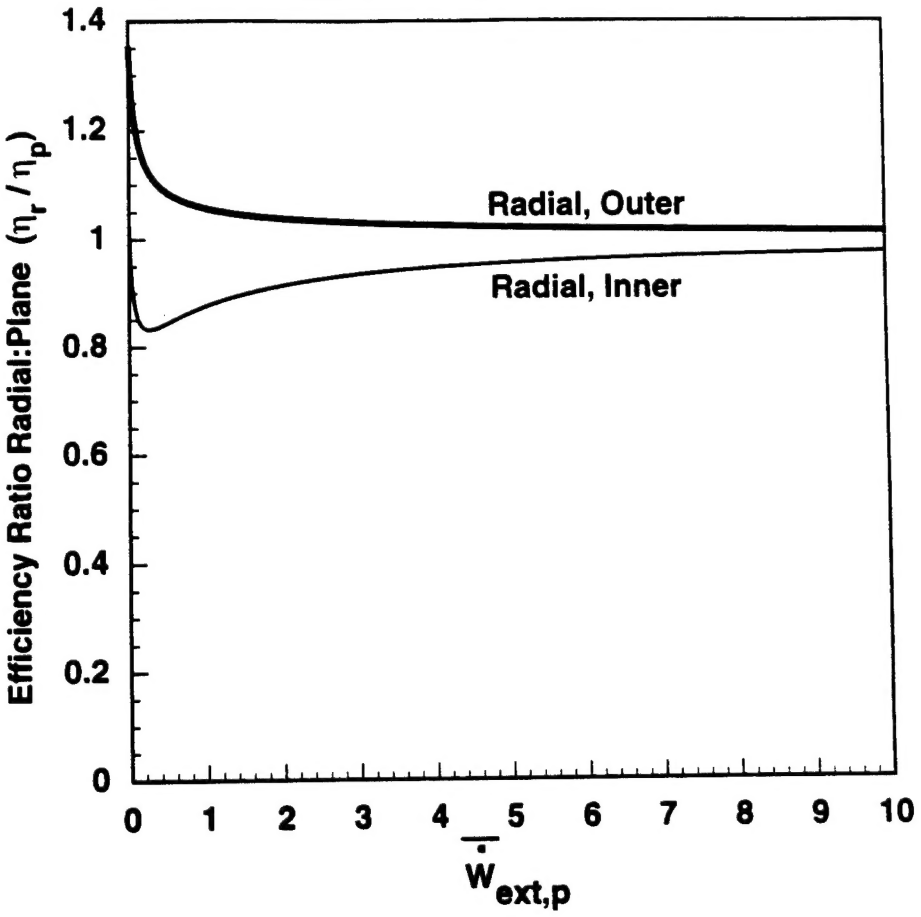
1.4
1.2
1
0.8
0.6
0.4
0.2
0
Efficiency Ratio Radial:Plane (η_r / η_p)
Radial, Outer
Radial, Inner
0
1
2
3
4
5
6
7
8
9
10
$\dot{W}_{ext,p}$